Mathematics in Applied Sciences and Engineering
Volume **4**, Number **4**, December **2023**, pp.**307-338**

https://ojs.lib.uwo.ca/mase
https://doi.org/10.5206/mase/16685

MULTISCALE MODELING APPROACH TO ASSESS THE IMPACT OF ANTIBIOTIC TREATMENT FOR COVID-19 ON MRSA TRANSMISSION AND ALTERNATIVE IMMUNOTHERAPY TREATMENT OPTIONS

TAYE FANIRAN, MATTHEW O. ADEWOLE, CATHERINE CHIROUZE, ANTOINE PERASSO, AND RALUCA EFTIMIE

Abstract. Methicillin-Resistant Staphylococcus Aureus (MRSA) infection can occur alongside or following COVID-19, which is a concern in healthcare settings. The effectiveness of antiviral treatments for COVID-19 depends on a functioning immune response, but antibiotics used for bacterial infections like MRSA can disrupt the immune response and reduce the effectiveness of antiviral treatments. The emergence of MRSA due to excessive antibiotic usage has led to the widespread use of vancomycin as an alternative treatment. Immunomodulatory antibiotics like azithromycin may also be considered. To study the dynamics of these coinfections, a multiscale model was developed. Parameter estimation and sensitivity analysis were performed, revealing influential parameters affecting the reproduction number. Numerical simulations showed that methicillin ($m = 1$) increases populations of co-infected cells (E_6), SARS-CoV-2 virus (V_2), and MRSA bacteria (B_N), and neutrophil populations (N_3) remain unaffected with methicillin. Increasing vancomycin effectiveness from 50% to 90% significantly reduces MRSA populations in individuals infected with MRSA (B_M) and individuals coinfected with COVID-19 and MRSA (B_N), with no notable changes on other cell populations. Similarly, enhancing the efficacy of immunomodulatory antibiotics (σ_3) results in an increased neutrophil population (N_3) without significant impacts on other cell populations. Higher β_3 values increased individuals coinfected with COVID-19 and MRSA (I_{CM}) at the between hosts, with no effect on other populations while within host cells infected with COVID-19 (E_2) significantly increased with higher β_3 and decreased with lower values. This underscores the coinfection rate's crucial role in promoting coinfected individuals, posing epidemiological concerns due to potentially severe health outcomes and acting as reservoirs for both pathogens (SARS-CoV-2 and MRSA bacteria). This study emphasizes the importance of continuous research, surveillance, and the development of effective strategies to combat the complexities of COVID-19 and MRSA coinfection.

1. Introduction

During the COVID-19 pandemic, prophylactic antibiotics such as methicillin, metronidazole, vancomycin, doxycline, clarithromycin, erythromycin, ciprofloxacin, and daptomycin were administered to patients to prevent the development of bacterial infections, as there were no antiviral drugs available at that time. However, the overuse and misuse of antibiotics led to the emergence of antibiotic-resistant strains of staphylococcus aureus, including methicillin-resistant staphylococcus aureus (MRSA) and vancomycin-resistant staphylococcus aureus [4]. Consequently, this led to the coinfection of COVID-19 and MRSA. In the context of this article, the term *coinfection* refers to staphylococcus aureus bacterial infection that can either occur concurrently with COVID-19 or develop as a subsequent infection following the primary SARS-CoV-2 infection. It encompasses both coinfection and superinfection. Coinfection

Received by the editors 19 July 2023; accepted 4 Decempber 2023; published online 16 December 2023.
2020 *Mathematics Subject Classification.* 92-4, 92-10.
Key words and phrases. Multiscale modeling; COVID-19 and MRSA coinfection; antibiotics; parameters estimation; sensitivity analysis; simulations.

generally refers to the simultaneous presence of multiple infectious agents, such as bacteria and viruses, in an individual. On the other hand, superinfection specifically refers to a secondary infection that occurs during the course of an existing infection, where the subsequent infection is caused by a different organism or strain [32]. Therefore, throughout this article, we will utilize the term *coinfection* to refer to both coinfection and superinfection, acknowledging the intertwined nature of the staphylococcus bacterial infection with COVID-19. By doing so, we aim to provide a comprehensive analysis of the bacterial aspect of COVID-19 and contribute to a deeper understanding of the multifaceted challenges posed by infectious diseases. Research conducted by [35] revealed that among 3,492 COVID-19 patients who were screened, 224 patients were positive to staphylococcus aureus and these strains were resistant to methicillin. Similarly, a study by [42] found a strong link between high levels of antibacterial drug consumption and the prevalence of antimicrobial resistance. MRSA is a type of staphylococcus aureus that no longer responds to antibiotics and has caused significant morbidity and mortality in health-care settings [22]. MRSA develops in staphylococcus aureus when the bacteria acquires a specific gene called mecA, which is found on the MRSA cassette chromosome mec element type A. The mecA gene encodes for Penicillin-Binding Protein 2a (PBP2a), a protein that has a lower affinity for beta-lactam antibiotics such as methicillin. When the mecA gene is present in staphylococcus aureus, it makes the bacteria resistant to beta-lactam antibiotics, including methicillin, reducing the effectiveness of these drugs against the bacteria. Despite exposure to these antibiotics, the resistant staphylococcus aureus strains can survive, grow, and reproduce. Over time, these resistant strains can become more prevalent in the host population, leading to the emergence of MRSA. It can spread by touching objects that have been contaminated by MRSA, such as towels, bandages, or medical equipment. MRSA can survive on surfaces for a significant amount of time, which makes it easier for it to spread in environments where many people are in close contact, such as hospitals or nursing homes [72]. MRSA is commonly found on the skin and respiratory tracts and has been identified as one of the main causes of lung infections in COVID-19 patients [10]. MRSA infections can be difficult to treat, as they are resistant to many commonly used antibiotics. Treatment typically involves the use of alternative antibiotics that are still effective against MRSA, such as vancomycin or daptomycin. Vancomycin has shown some effectiveness in slowing the growth of MRSA in a host [50]. SARS-CoV-2, the virus responsible for COVID-19, primarily targets lung epithelial cells. Given that COVID-19 treatment can promote the growth of MRSA and both pathogens infect lung epithelial cells, it is necessary to investigate the dynamics of co-infection between the two diseases [12],[48]. Co-infected patients commonly experience symptoms such as fever, cough, dyspnea, diarrhea, and vomiting [5].

The immune system's response is crucial for fighting off bacterial and viral infections. The first line of defense consists of innate immunity, which includes macrophages, neutrophils, dendritic cells, and natural killer cells. Macrophages identify invading pathogen and release cytokines that recruit other immune cells to attack the pathogen. Neutrophils are the primary defenders against Staphylococcus aureus infections, rapidly attacking the bacteria at the site of infection [31]. These immune cells are highly activated in COVID-19 patients [52]. Unlike dendritic cells, neutrophils are highly effective at breaking down antigens coated by them [77]. They are also the most abundant circulating white blood cells. While neutrophils are primarily known for their role in combating bacterial infections, they also play an important role in the response to viral infections [54]. However, the rise of antibiotic-resistant bacteria threatens the effectiveness of antibiotic treatments for staphylococcus infections. Therefore, administering immunomodulatory antibiotics like azithromycin, clarithromycin, and fluoroquinolones (such as ciprofloxacin and levofloxacin) could be a useful alternative approach [73],[63],[66]. These antibiotics enhance the innate immune response, particularly neutrophil function, by boosting its capacity

to kill bacteria [63]. They can also interact with human defenses to reduce the virulence of intracellular bacterial pathogens like staphylococcus aureus, making them more vulnerable to phagocytosis and elimination by the immune system [19],[3]. This therapeutic strategy could be beneficial in fighting infectious diseases [36].

The efficacy of antiviral drugs such as remdesivir and molnupiravir, in treating COVID-19 relies on the proper functioning of the immune response. However, the use of antibiotics such as methicillin, nafcillin, cefazolin and dicloxacillin can indirectly affect the immune response, which is crucial for fighting viral infections [69]. Consequently, it is essential to comprehend the influence of methicillin on the dynamics of coinfection and other antiviral therapies for effective management. Disruption of the microbiome, which includes beneficial bacteria that contribute to immune function, can occur due to the use of these antibiotics [49] [62]. The microbiome refers to the diverse communities of microorganisms in the body, playing a vital role in overall health and immune function. Within the microbiome, beneficial bacteria contribute to immune system development and function. Antibiotics, including those used for staphylococcus bacterial infections, can disrupt the microbiome by targeting both harmful and beneficial bacteria. The microbiome interacts extensively with the immune system, influencing its development and response to infections. Beneficial bacteria in the microbiome support immune cell production, regulate immune signaling, and aid in pathogen defense. Antibiotic-induced disruption of the microbiome can compromise these interactions, potentially compromising immune function. In the context of viral infections like COVID-19, where immune response is crucial, microbiome disruption by antibiotics can lead to dysregulated immune responses, impacting the body's ability to mount an effective antiviral defense [37]. These effects can have consequences for the overall outcome of the coinfection, including the severity of symptoms, the progression of the diseases, and the effectiveness of the treatments.

Several studies have used mathematical models to evaluate the transmission dynamics of COVID-19, MRSA, and the progression of SARS-CoV-2 within humans and in-host MRSA bacteria. Additionally, the co-infection dynamics between bacteria and viruses have also been explored through mathematical modeling [41],[58],[24],[25],[26],[6], [30],[8],[9],[15], [13],[74],[18]. For instance, Zhou et al [80] proposed a mathematical model of SARS-CoV-2 and bacteria coinfection considering SARS-CoV-2, bacteria, neutrophils and lymphocytes. Mekonen et al [53] studied a coinfection dynamics between mycobacterium bacteria and SARS-CoV-2 using a system of nonlinear ODE. Perez et al [64] proposed an epidemic model to explore the dynamics of co-infection between COVID-19 and bacterial pneumonia. Community-acquired and hospital-acquired infection ways for pneumonia were considered in their model. Cheng et al [14] formulated a mathematical model that simulates the risk of developing pneumonia and chronic obstructive pulmonary disease (COPD) after being infected with both influenza A virus and streptococcus pneumoniae by considering factors such as age, smoking history, and vaccination status. Mbabazi et al [57] proposed a mathematical model that simulates the within-host co-infection of influenza A virus and pneumococcus. The model took into account various factors such as viral and bacterial replication rates, immune response, and antibiotic treatment.

Previous studies have examined viral and bacterial infections, as well as some models of coinfection between them, either at the immunological or epidemiological level. However, the current study takes a novel approach by investigating the effect of coinfection on both levels simultaneously, including a specific strain of antibiotic-resistant bacteria, methicillin-resistant staphylococcus aureus (MRSA), which has not been previously considered. Given the rising incidence of antibiotic-resistant bacteria and the shortage of novel antibiotic drugs, our study seeks to investigate the consequences of administering antibiotic (methicillin) for COVID-19 on the transmission of MRSA and also to explore substitute treatment options, including immunotherapy. Moreover, since the use of antibiotics such as methicillin,

nafcillin, cefazolin and dicloxacillin can indirectly affect the immune response, which is crucial for fighting viral infections like COVID-19, and which in turn can have consequences for the overall outcome of the COVID-19-MRSA coinfection, including the severity of symptoms, the progression of the diseases, and the effectiveness of the treatments [69], understanding the specific impact of methicillin on the coinfection dynamics becomes crucial. The study poses three research questions: (i) How can a deterministic differential equation coinfection model be developed to link the between-host and within-host scales? (ii) How does the presence of methicillin affect the dynamics of co-infection of SARS-CoV-2 and MRSA bacteria? (iii) What are the most effective treatment strategies, including combinations of vancomycin and immunomodulatory antibiotics (e.g., azithromycin), for managing co-infection with COVID-19 and methicillin-resistant Staphylococcus aureus (MRSA), considering the impact on both within-host dynamics and population-level spread? To address these research questions, we develop a multiscale model that integrates the between-host and within-host dynamics of the coinfection. The model comprises various compartments, each representing a distinct aspect of the coinfection process.

At the between-host scale, we consider susceptible individuals, those infected with COVID-19, those infected with MRSA, individuals with a co-infection of COVID-19 and MRSA, isolated individuals, environmental virus, environmental MRSA, and recovered individuals. At the within-host scale for COVID-19, we compartmentalize the model into uninfected cells, COVID-19 infected cells, within-host SARS-CoV-2, and the population of neutrophils. Similarly, for MRSA, we categorize the within-host scale into uninfected cells, MRSA-infected cells, the population of Methicillin-Sensitive Staphylococcus Aureus (MSSA), the population of MRSA, and the population of neutrophils. For individuals with a co-infection of COVID-19 and MRSA, the within-host scale includes COVID-19-MRSA uninfected cells, COVID-19-MRSA co-infected cells, within-host SARS-CoV-2, the population of MSSA, the population of MRSA, and the population of neutrophils. By including these compartments in a single model, we can capture the interplay between different scales and gain insights into the complex interactions occurring during coinfection. This approach provides insights into the dynamics of each pathogen individually, including how they spread, interact with the host immune response, and affect disease progression. By studying each pathogen independently, we establish a foundation of knowledge about their behavior before investigating the combined effects of coinfection. This comprehensive analysis enables a deeper understanding of the individual dynamics, infection mechanisms, and the complex interactions between COVID-19 and MRSA. Ultimately, this approach enhances our ability to accurately represent real-world coinfection scenarios and gain a more subtlety understanding of their complexities.

2. Materials and Methods

2.1. **Between-host dynamics.** The between-host dynamics is separated into various categories, including susceptible individuals (S_H), those infected with COVID-19 (I_C), those infected with MRSA (I_M), individuals with a co-infection of COVID-19 and MRSA (I_{CM}), isolated individuals (J), environmental virus (V_E), environmental MRSA (B_E), and recovered individuals (R_H).

Susceptible individuals S_H, are recruited at a rate (Λ). These individuals can become infected with COVID-19 by coming into contact with those who are infected with COVID-19 alone I_C, or co-infected with both COVID-19 and MRSA I_{CM} or by coming into contact with environmental virus at a rate α_3 [23], [53] . The probability of successfully becoming infected is denoted by β_1. Additionally, susceptible individuals can also become infected with MRSA by coming into contact with those who are infected with MRSA alone I_M, or co-infected with both COVID-19 and MRSA. The probability of successfully becoming infected is denoted by (β_2). Furthermore, susceptible individuals can also become co-infected with both COVID-19 and MRSA by coming into contact with individuals who are already co-infected. The probability of successfully becoming co-infected is denoted by (β_3). The parameter (α_1) represents

the fraction of susceptible individuals who come into contact with individuals co-infected with COVID-19 and MRSA and will become infected with COVID-19, while (α_2) represents the fraction of susceptible individuals who come into contact with individuals co-infected with COVID-19 and MRSA and will become infected with MRSA. Lastly, susceptible individuals are subject to a death rate of (μ). Thus, the changes in the susceptible individuals are described by the following equation:

$$\begin{aligned}\frac{dS_H}{dt} &= \Lambda - \beta_1(V_1)S_H I_C - \alpha_1\beta_1(V_2)S_H I_{CM} - \beta_2(B_1+B_M)S_H I_M - \alpha_2\beta_2(B_2+B_N)S_H I_{CM} - \\ &\quad (1-\alpha_1)(1-\alpha_2)\beta_3(V_2, B_2+B_N)S_H I_{CM} - \alpha_3 S_H V_E - \mu S_H \end{aligned} \tag{2.1}$$

The number of individuals infected with COVID-19, denoted as I_C [7], can increase if susceptible individuals come into contact with either individuals infected with COVID-19 only (I_C) or individuals co-infected with both COVID-19 and MRSA (I_{CM}) with a probability of successful infection denoted as (β_1). The fraction of susceptible individuals who come into contact with I_{CM} and are infected with COVID-19 only is denoted as (α_1). Additionally, individuals infected with COVID-19 can increase if susceptible individuals come into contact with the environmental virus V_E at a rate α_3. Conversely, the population of infected individuals will decrease due to factors such as recovery rate (ν), isolation rate (a), disease-induced death rate (δ_1), natural death rate (μ), and the rate at which I_C contacts I_M, denoted as β_4. The dynamics is given by

$$\frac{dI_C}{dt} = \beta_1(V_1)S_H I_C + \alpha_1\beta_1(V_2)S_H I_{CM} + \alpha_3 S_H V_E - \beta_4(B_1+B_M)I_C I_M - (\nu + a + \delta_1 + \mu)I_C. \tag{2.2}$$

The population of individuals infected with MRSA, denoted as I_M [33], results from contact between susceptible individuals and those infected with either MRSA only (I_M) or individuals co-infected with both COVID-19 and MRSA (I_{CM}), with a probability of success infection denoted as (β_2). The fraction of susceptible individuals who come into contact with I_{CM} and are infected with MRSA only is denoted as (α_2). However, the population of individuals infected with MRSA will decrease due to factors such as probability (β_5) that individuals infected with MRSA I_M, contact individuals infected with COVID-19, I_C, and a rate (α_6) at which individuals infected with MRSA I_M, contact the environmental virus, V_E, recovery rate (r), isolation rate (b), disease-induced death rate (δ_2), and natural death rate (μ). The dynamics is given by

$$\frac{dI_M}{dt} = \beta_2(B_1+B_M)S_H I_M + \alpha_2\beta_2(B_2+B_N)S_H I_{CM} - \beta_5(V_1)I_M I_C - \beta_6 I_M V_E - (r+b+\delta_2+\mu)I_M. \tag{2.3}$$

The population of individuals co-infected with COVID-19 and MRSA, denoted as I_{CM} [68], is generated when susceptible individuals are infected with both diseases as a result of contact with individuals co-infected with COVID-19 and MRSA. The population of individuals co-infected with COVID-19 and MRSA increases with the probability that individuals infected with COVID-19 (I_C) come into contact with individuals infected with MRSA (I_M), and with the probability that individuals infected with MRSA come into contact with individuals infected with COVID-19. The population of individuals co-infected with COVID-19 and MRSA also increases when individuals infected with MRSA (I_M) come into contact with the environmental virus (V_E) at a rate β_6. The population of individuals co-infected with COVID-19 and MRSA will decrease due to factors such as recovery rate (ω), isolation rate (g), disease-induced death rate (δ_3), and natural death rate (μ). The dynamics is given by

$$\begin{aligned}\frac{dI_{CM}}{dt} &= (1-\alpha_1)(1-\alpha_2)\beta_3(V_2, B_2+B_N)S_H I_{CM} + \beta_4(B_1+B_M)I_C I_M + \\ &\quad \beta_5(V_1)I_M I_C + \beta_6 I_M V_E - (\omega + l + \delta_3 + \mu)I_{CM} \end{aligned} \tag{2.4}$$

The population of isolated individuals results from the isolation of individuals infected with COVID-19 [29], individuals infected with MRSA [16], and individuals co-infected with COVID-19 and MRSA

at rates denoted as (a), (b), and (l) respectively. However, the population of isolated individuals will decrease due to factors such as recovery rate (n), disease-induced death rate (δ_4), and natural death rate (μ). The dynamics is given by

$$\frac{dJ}{dt} = aI_C + bI_M + lI_{CM} - (n + \delta_4 + \mu)J. \tag{2.5}$$

The environmental virus population occurs due to the shedding of virus by individuals who are infected with COVID-19 alone or those who are co-infected with COVID-19 and MRSA [82], [44]. The shedding rates for these two groups are denoted by (p_1) and (p_2), respectively. A fraction (τ_1) of those who are co-infected with COVID-19 and MRSA and shedding the virus contribute to the environmental virus population. Additionally, the rate of virus clearance from the environment is denoted by (h_1). The dynamics is given by

$$\frac{dV_E}{dt} = p_1 I_C + p_2\tau_1 I_{CM} - h_1 V_E. \tag{2.6}$$

The environmental bacteria population occurs due to the shedding of bacteria by individuals who are infected with MRSA alone or those who are co-infected with COVID-19 and MRSA [82], [44]. The shedding rates for these two groups are denoted by (λ_1) and (λ_2), respectively. Also, a fraction (τ_2) of those who are co-infected with COVID-19 and MRSA and shedding the MRSA contribute to the environmental bacteria population. Additionally, the rate of bacterial clearance from the environment is denoted by (h_2). The dynamics is given by

$$\frac{dB_E}{dt} = \lambda_1 I_M + \lambda_2\tau_2 I_{CM} - h_2 B_E. \tag{2.7}$$

The recovered population is generated as a result of individuals who have recovered from COVID-19 only with a recovery rate (ν), those who have recovered from MRSA only with a recovery rate (r), those who have recovered from co-infection of COVID-19 and MRSA with a recovery rate (ω), and isolated individuals who have recovered with a recovery rate (n). The population size declines due to natural death at a rate of (μ). The dynamics is given by

$$\frac{dR}{dt} = \nu I_C + rI_M + \omega I_{CM} + nJ - \mu R. \tag{2.8}$$

The full between-host dynamics is given as:

$$\begin{aligned}\frac{dS_H}{dt} &= \Lambda - \beta_1(V_1)S_H I_C - \alpha_1\beta_1(V_2)S_H I_{CM} - \beta_2(B_1 + B_M)S_H I_M - \alpha_2\beta_2(B_2 + B_N)S_H I_{CM} \\ &\quad - (1-\alpha_1)(1-\alpha_2)\beta_3(V_2, B_2 + B_N)S_H I_{CM} - \alpha_3 S_H V_E - \mu S_H,\end{aligned} \tag{2.9}$$

$$\frac{dI_C}{dt} = \beta_1(V_1)S_H I_C + \alpha_1\beta_1(V_2)S_H I_{CM} + \alpha_3 S_H V_E - \beta_4(B_1 + B_M)I_C I_M - (\nu + a + \delta_1 + \mu)I_C, \tag{2.10}$$

$$\frac{dI_M}{dt} = \beta_2(B_1 + B_M)S_H I_M + \alpha_2\beta_2(B_2 + B_N)S_H I_{CM} - \beta_5(V_1)I_M I_C - \beta_6 I_M V_E - (r + b + \delta_2 + \mu)I_M, \tag{2.11}$$

$$\begin{aligned}\frac{dI_{CM}}{dt} &= (1-\alpha_1)(1-\alpha_2)\beta_3(V_2, B_2 + B_N)S_H I_{CM} + \beta_4(B_1 + B_M)I_C I_M + \beta_5(V_1)I_M I_C \\ &\quad + \beta_6 I_M V_E - (\omega + l + \delta_3 + \mu)I_{CM},\end{aligned} \tag{2.12}$$

$$\frac{dJ}{dt} = aI_C + bI_M + lI_{CM} - (n + \delta_4 + \mu)J, \tag{2.13}$$

$$\frac{dV_E}{dt} = p_1 I_C + p_2 \tau_1 I_{CM} - h_1 V_E, \tag{2.14}$$

$$\frac{dB_E}{dt} = \lambda_1 I_M + \lambda_2 \tau_2 I_{CM} - h_2 B_E, \tag{2.15}$$

$$\frac{dR}{dt} = \nu I_C + r I_M + \omega I_{CM} + nJ - \mu R. \tag{2.16}$$

2.2. **Within-host dynamics.** The within-host dynamics is subdivided into within-host scale for COVID-19 infected individuals [88], within-host scale for MRSA infected individuals [50] and within-host scale for individuals with a co-infection of COVID-19 and MRSA. The within-host scale for COVID-19 infected individuals is compartmentalized into uninfected cells (E_1), COVID-19 infected cells (E_2), within-host SARS-CoV-2 (V_1) and population of neutrophils N_1. Similarly, the within-host scale for MRSA infected individuals is divided into uninfected cells (E_3), MRSA-infected cells (E_4), population of Methicillin-Sensitive Staphylococcus Aureus (MSSA) (B_1), population of MRSA (B_M) and population of neutrophils N_2. Lastly, the within-host scale for individuals with a co-infection of COVID-19 and MRSA is separated into COVID-19-MRSA uninfected cells (E_5), COVID-19-MRSA co-infected cells (E_6), within-host SARS-CoV-2 (V_2), population of MSSA (B_2), population of MRSA (B_N) and population of neutrophils N_3.

At the within-host scale for COVID-19 infected individuals, uninfected cells E_1 become infected when they encounter the SARS-CoV-2 virus V_1 at a rate (ψ_1) and the population size decreases due to natural death rate (ρ_1). The within-host SARS-CoV-2 population increases and replicates itself within the COVID-19 infected cells at a rate (κ_1). The population reduces due to clearance rate (e_1) of the virus by neutrophils and virus death at a rate (ρ_2) [77], [54]. Additionally, the rate at which neutrophils are produced is determined by the recruitment rate (π_1), while the growth of the neutrophil population is influenced by the presence of an infection and the effectiveness of immunomodulatory antibiotics [63], represented by (σ_1). The population decreases further due to death of neutrophils at a rate (ϕ_1). The dynamics at within-host scale of SARS-CoV-2-infected individuals is given by:

$$\frac{dE_1}{dt} = \varepsilon_1 - \psi_1 E_1 V_1 - \rho_1 E_1, \tag{2.17}$$

$$\frac{dE_2}{dt} = \psi_1 E_1 V_1 - \rho_1 E_2, \tag{2.18}$$

$$\frac{dV_1}{dt} = f_1 V_E + \kappa_1 E_2 - e_1 N_1 V_1 - \rho_2 V_1, \tag{2.19}$$

$$\frac{dN_1}{dt} = \pi_1 + \sigma_1 N_1 E_2 - \phi_1 N_1. \tag{2.20}$$

In individuals infected with MRSA at the within-host scale, the uninfected cells in the infected site I_M are constantly replenished at a rate (ε_2), and they also naturally die at a rate (φ). These uninfected cells in I_M can become infected at a rate of ψ_2. The expressions $(1-\theta)\gamma_1 B_1 [1-(B_1+B_M)/K_1]$ and $(1-\theta)\gamma_1 B_M [1-(B_1+B_M)/K_1]$ denote the logistic growth of MSSA and MRSA where B_1 and B_M denote the number of MSSA and MRSA bacteria, θ represents the efficacy of vancomycin, a drug used to treat MRSA infections. A value of $\theta = 1$ indicates complete effectiveness of vancomycin, while $\theta = 0$ implies no effectiveness at all, and $B_1 + B_M$ denotes the total number of staphylococcus aureus respectively [50]. It is assumed that MSSA and MRSA bacteria grow logistically with a growth rate of γ_1 and a carrying capacity of K_1 [50]. Within I_M, e_2 and e_3 signify the rates at which neutrophils clear MSSA and MRSA. The term $sB_1 m$ describes the rate at which MSSA switches to MRSA in the presence of methicillin, where m is a binary variable indicating the presence ($m = 1$) or absence ($m = 0$) of methicillin. As the population of MSSA increases, so does the rate of switching to MRSA and there is

death of MSSA and MRSA at a rate (d_1). Further, the rate at which neutrophils grow depends on the rate of recruiting new neutrophils before administering immunomodulatory antibiotics, which is shown by the symbol (π_2). When there is an infection, the number of neutrophils in the body increases as a response, and the effectiveness of immunomodulatory antibiotics, denoted as (σ_2), also plays a role. Furthermore, due to cell death, the population of neutrophils declines naturally at a rate of (ϕ_2). The dynamics is given by

$$\begin{aligned}
\frac{dE_3}{dt} &= \varepsilon_2 - \psi_2 E_3(B_1 + B_M) - \varphi E_3, && (2.21)\\
\frac{dE_4}{dt} &= \psi_2 E_3(B_1 + B_M) - \varphi E_4. && (2.22)\\
\frac{dB_1}{dt} &= f_2 B_E + (1-\theta)\gamma_1 B_1\left(1 - \frac{B_1 + B_M}{K_1}\right) - e_2 N_2 B_1 - sB_1 m - d_1 B_1, && (2.23)\\
\frac{dB_M}{dt} &= (1-\theta)\gamma_1 B_M\left(1 - \frac{B_1 + B_M}{K_1}\right) + sB_1 m - e_3 N_2 B_M - d_1 B_M, && (2.24)\\
\frac{dN_2}{dt} &= \pi_2 + \sigma_2 N_2 E_4 - \phi_2 N_2. && (2.25)
\end{aligned}$$

The co-infection of COVID-19 and MRSA within-host dynamics involves the infection of uninfected cells (E_5) by within-host staph aureus and SARS-CoV-2 at rates (ψ_3) and (ψ_4) respectively, and their subsequent death at a rate (ζ). The production rate of virus (κ_2) in I_{CM} results in the generation of within-host SARS-CoV-2, which is cleared by neutrophils at a rate (z_1) and the virus dies at a rate (ρ_3). For the in-host staph aureus, the logistic growths of MSSA and MRSA are represented by $(1-\theta)\gamma_2 B_2\left[1-(B_2+B_N)/K_2\right]$ and, $(1-\theta)\gamma_2 B_N\left[1-(B_2+B_N)/K_2\right]$ with efficacy of vancomycin θ, a growth rate of γ_2 and a carrying capacity of K_2 [50]. Within I_{CM}, z_2 and z_3 are used to signify the rates at which neutrophils clear MSSA and MRSA. The term uB_2m describes the rate at which MSSA transforms into MRSA in the presence of methicillin, where m is a binary variable indicating the presence or absence of methicillin. As the population of MSSA increases, so does the rate of switching to MRSA. The parameter d_2 represents the death rate of MSSA and MRSA in I_{CM}. Lastly, the growth rate of neutrophils is contingent upon the rate at which new neutrophils are recruited prior to the use of immunomodulatory antibiotics represented by the symbol π_3. The population of neutrophils increases in response to an infection and the administration of immunomodulatory antibiotic (azithromycin), with the efficacy of the antibiotics denoted by (σ_3) being a contributing factor. In addition, the neutrophil population naturally decreases at a rate of (ϕ_3) due to cell death. The dynamics is given as

$$\begin{aligned}
\frac{dE_5}{dt} &= \varepsilon_3 - \psi_3 E_5(B_2 + B_N) - \psi_4 E_5 V_2 - \zeta E_5, && (2.26)\\
\frac{dE_6}{dt} &= \psi_3 E_5(B_2 + B_N) - \psi_4 E_5 V_2 - \zeta E_6, && (2.27)\\
\frac{dV_2}{dt} &= f_3 V_E + \kappa_2 E_6 - z_1 N_3 V_2 - \rho_3 V_2, && (2.28)\\
\frac{dB_2}{dt} &= f_4 B_E + (1-\theta)\gamma_2 B_2\left(1 - \frac{B_2 + B_N}{K_2}\right) - z_2 N_3 B_2 - uB_2 m - d_2 B_2, && (2.29)\\
\frac{dB_N}{dt} &= (1-\theta)\gamma_2 B_N\left(1 - \frac{B_2 + B_N}{K_2}\right) + uB_2 m - z_3 N_3 B_N - d_2 B_N, && (2.30)\\
\frac{dN_3}{dt} &= \pi_3 + \sigma_3 N_3 E_6 - \phi_3 N_3. && (2.31)
\end{aligned}$$

The full within-host dynamics is given as:

$$\frac{dE_1}{dt} = \varepsilon_1 - \psi_1 E_1 V_1 - \rho_1 E_1, \tag{2.32}$$

$$\frac{dE_2}{dt} = \psi_1 E_1 V_1 - \rho_1 E_2, \tag{2.33}$$

$$\frac{dV_1}{dt} = f_1 V_E + \kappa_1 E_2 - e_1 N_1 V_1 - \rho_2 V_1, \tag{2.34}$$

$$\frac{dN_1}{dt} = \pi_1 + \sigma_1 N_1 E_2 - \phi_1 N_1, \tag{2.35}$$

$$\frac{dE_3}{dt} = \varepsilon_2 - \psi_2 E_3 (B_1 + B_M) - \varphi E_3, \tag{2.36}$$

$$\frac{dE_4}{dt} = \psi_2 E_3 (B_1 + B_M) - \varphi E_4, \tag{2.37}$$

$$\frac{dB_1}{dt} = f_2 B_E + (1-\theta)\gamma_1 B_1 \left(1 - \frac{B_1 + B_M}{K_1}\right) - e_2 N_2 B_1 - s B_1 m - d_1 B_1, \tag{2.38}$$

$$\frac{dB_M}{dt} = (1-\theta)\gamma_1 B_M \left(1 - \frac{B_1 + B_M}{K_1}\right) + s B_1 m - e_3 N_2 B_M - d_1 B_M, \tag{2.39}$$

$$\frac{dN_2}{dt} = \pi_2 + \sigma_2 N_2 E_4 - \phi_2 N_2, \tag{2.40}$$

$$\frac{dE_5}{dt} = \varepsilon_3 - \psi_3 E_5 (B_2 + B_N) - \psi_4 E_5 V_2 - \zeta E_5, \tag{2.41}$$

$$\frac{dE_6}{dt} = \psi_3 E_5 (B_2 + B_N) + \psi_4 E_5 V_2 - \zeta E_6, \tag{2.42}$$

$$\frac{dV_2}{dt} = f_3 V_E + \kappa_2 E_6 - z_1 N_3 V_2 - \rho_3 V_2, \tag{2.43}$$

$$\frac{dB_2}{dt} = f_4 B_E + (1-\theta)\gamma_2 B_2 \left(1 - \frac{B_2 + B_N}{K_2}\right) - z_2 N_3 B_2 - u B_2 m - d_2 B_2, \tag{2.44}$$

$$\frac{dB_N}{dt} = (1-\theta)\gamma_2 B_N \left(1 - \frac{B_2 + B_N}{K_2}\right) + u B_2 m - z_3 N_3 B_N - d_2 B_N, \tag{2.45}$$

$$\frac{dN_3}{dt} = \pi_3 + \sigma_3 N_3 E_6 - \phi_3 N_3. \tag{2.46}$$

TABLE 1. Summary of the parameters

Parameter	Meaning	Value	Reference
β_1	Infection rate of COVID-19	$4.791983999900046 \times 10^{-9}$ individual^{-1} day^{-1}	Data fitting
β_4	Rate at which I_C contacts I_M	$1.482880000000000 \times 10^{-10}$ individual^{-1} day^{-1}	Data fitting
a	Isolation rate of I_C	0.2797 day^{-1}	Data fitting
f_1^0	Contribution rate to the in-host virus from the environment within I_C	0.0288 day^{-1}	Data fitting
p_1	Shedding rate of virus by I_C	1.4623 virus individual^{-1} day^{-1}	Data fitting
p_2	Shedding rate of virus by I_{CM}	3.9809 virus individual^{-1} day^{-1}	Data fitting
α_3	Rate at which S_H contacts environmental virus (V_E)	10^{-10} individual^{-1} day^{-1}	Data fitting
β_2	Infection rate of MRSA	1.6854×10^{-10} individual^{-1} day^{-1}	Estimated from [34]
β_5	Rate at which I_M contacts I_C	1.0477×10^{-9} individual^{-1} day^{-1}	Estimated from [34]
Λ	Recruitment rate of humans	2240.7 individual^{-1} day^{-1}	Estimated from [28],[86]
α_1	Fraction of S_H who have contact with I_{CM} but will be infected with COVID-19 only	0.55	Estimated from [34]

Continued on next page

Table 1 – continued from previous page

Parameter	Meaning	Value	Reference
α_2	Fraction of S_H who have contact with I_{CM} but will be infected with MRSA only	0.55	Assumed
β_6	Rate at which I_M contacts environmental virus (V_E)	10^{-8} individual^{-1} day^{-1}	Assumed
β_3	Co-infection rate of COVID-19 and MRSA	10^{-9} individual^{-1} day^{-1}	Estimated from [1]
μ	Natural mortality rate	0.000033 day^{-1}	[28]
ν	Recovery rate of I_C	$\frac{1}{25}$ day^{-1}	Estimated from [47]
δ_1	Disease-induced death rate of I_C	0.001 day^{-1}	[88]
r	Recovery rate of I_M	0.006 day^{-1}	[15]
b	Isolation rate of I_M	0.0001460 day^{-1}	Estimated from [10]
δ_2	Disease-induced death rate of I_M	0.000285 day^{-1}	[1]
ω	Recovery rate of I_{CM}	$\frac{1}{100}$ day^{-1}	Estimated from [47]
l	Isolation rate of I_{CM}	0.001 day^{-1}	Estimated from [10]
δ_3	Disease-induced death rate of I_{CM}	$\frac{1}{30}$ day^{-1}	[1]
n	Recovery rate of isolated individuals	0.0815 day^{-1}	[6]
δ_4	Disease-induced death rate of isolated individuals	6.847×10^{-4} day^{-1}	[6]
τ_1	Fraction of I_{CM} who sheds SARS-CoV-2	0.5	[88]
τ_2	Fraction of I_{CM} who sheds MRSA	0.01	Estimated from [65]
λ_1	Shedding rate of bacteria by I_M	1.729 bacteria individual^{-1} day^{-1}	Estimated from [65]
λ_2	Shedding rate of bacteria by I_{CM}	1.995 bacteria individual^{-1} day^{-1}	Estimated from [65]
h_1	Rate of virus clearance in the environment	0.3 day^{-1}	[88]
h_2	Rate of bacterial clearance in the environment	0.3 day^{-1}	[38]
ε_1	Constant regeneration rate of COVID-19 uninfected cells	$E_1^0 \times \rho_1$ cells ml^{-1} min^{-1}	[88]
ψ_1	Infection rate of COVID-19 uninfected cells	10^{-8} day^{-1}	Estimated from [88]
ρ_1	Death rate of COVID-19 uninfected cells inside I_C	0.01 day^{-1}	[88]
f_2^0	Contribution rate to the in-host bacteria from the environment within I_M	10^{-4} day^{-1}	Estimated from [88]
f_3^0	Contribution rate to the in-host virus from the environment within I_C	0.03 day^{-1}	Estimated from [88]
f_4^0	Contribution rate to the in-host bacteria from the environment within I_{CM}	10^{-4} day^{-1}	Estimated from [88]
q_0, g_0	Factors that measure how the transmission rate changes with viral load and bacteria	10^{-15}	Assumed
κ_1	Production rate of SARS-CoV-2 in I_C	0.24 copies cell^{-1} day $^{-1}$	[13]
κ_2	Production rate of virus from co-infected cells in I_{CM}	0.1copies cell^{-1} day^{-1}	Estimated from [13]
ρ_2	Death rate of virus within I_C class	0.230 day^{-1}	[88]
ε_2	Constant regeneration rate of MRSA uninfected cells	$E_3^0 \times \varphi$ day^{-1}	[15]
ε_3	Constant regeneration rate of COVID-MRSA uninfected cells	$E_5^0 \times \zeta$ day^{-1}	Estimated from [15]
ψ_2	Infection rate of MRSA uninfected cells by staph aureus	$(10^{-6} - 10^{-2})$ ml h^{-1} cfu^{-1}	Estimated from [50]
ψ_3	Infection rate of COVID-19-MRSA uninfected cells by staph aureus	0.000000024 ml h^{-1} cfu^{-1}	Estimated from [50]
ψ_4	Infection rate of COVID-19-MRSA uninfected cells by SARS-CoV-2	10^{-8} ml copies^{-1} day^{-1}	Estimated from [50]
φ	Natural death rate of MRSA uninfected cells in I_M	0.04 day^{-1}	[50]
γ_1	Intrisic growth rate of staph aureus in the absence of methicillin in I_M	0.1514304 day^{-1}	[50]
γ_2	Intrisic growth rate of staph aureus in the absence of methicillin in I_{CM}	0.1514304 day^{-1}	[50]
m	Methicillin	$\{0, 1\}$	Estimated from [50]
K_1	Carrying capacity of the host for MSSA in I_M	1×10^8 cfu a.u^{-1}	[50]
K_2	Carrying capacity of the host for MSSA in I_{CM}	1×10^8 cfu a.u^{-1}	[50]
d_1	Decay rate of MRSA bacteria in I_M	0.07 day^{-1}	Assumed
s	Switching rate from MSSA to MRSA in the presence of methicillin within I_M	0.0758932 day^{-1}	Estimated from [50]

Continued on next page

Table 1 – continued from previous page

Parameter	Meaning	Value	Reference
u	Switching rate from MSSA to MRSA in the presence of methicillin within I_{CM}	0.0758932 day^{-1}	Estimated from [50]
e_1	Clearance rate of virus in I_C by neutrophils	0.0000024 day^{-1}	Estimated from [13]
e_2	Clearance rate of MSSA in I_M by neutrophils	0.000024 ml N cell^{-1} day^{-1}	Estimated from [50]
e_3	Clearance rate of MRSA in I_M by neutrophils	0.0000024 ml N cell^{-1} day^{-1}	[50]
z_1	Clearance rate of virus in I_{CM} by neutrophils	0.0000024 ml N cell^{-1} day^{-1}	[50]
z_2	Clearance rate of MSSA in I_{CM} by neutrophils	0.000024 ml cfu^{-1} day^{-1}	Estimated from [50]
z_3	Clearance rate of MRSA in I_{CM} by neutrophils	0.0000024 ml cfu^{-1} day^{-1}	[50]
σ_1	Effectiveness of Azithromycin in enhancing neutrophils in I_C	10^{-7} ml N cell^{-1} day^{-1}	[50]
σ_2	Effectiveness of Azithromycin in enhancing neutrophils in I_M	10^{-7} ml N cell^{-1} day^{-1}	[50]
σ_3	Effectiveness of Azithromycin in enhancing neutrophils in I_{CM}	10^{-7} ml N cell^{-1} day^{-1}	[50]
ϕ_1	Removal rate of neutrophils in I_C from the blood stream	$\frac{1}{5.4}$ day^{-1}	Estimated from [60]
ϕ_2	Removal rate of neutrophils in I_M from the blood stream	$\frac{1}{5.4}$ day^{-1}	Estimated from [60]
ϕ_3	Removal rate of neutrophils in I_{CM} from the blood stream	$\frac{1}{5.4}$ day^{-1}	Estimated from [60]
θ	Efficacy of vancomycin	$(0-1)$	[50]
ζ	Natural death rate of COVID-19-MRSA uninfected cells in I_{CM}	0.01 day^{-1}	Estimated from [88]
ρ_3	Death rate of V_2 in I_{CM}	0.01 day^{-1}	Estimated from [88]
d_2	Decay rate of MRSA in I_{CM}	0.07 min^{-1}	Estimated from [87]
π_1	Production rate of neutrophils in I_C	3.2×10^2 cell day^{-1}	Estimated from [13]
π_2	Production rate of neutrophils in I_M	3.2×10^2 cell day^{-1}	Estimated from [13]
π_3	Production rate of neutrophils in I_{CM}	3.2×10^2 cell day^{-1}	Estimated from [13]

Remark 2.2.1. In the within-host scale, we consider three distinct populations of uninfected cells denoted as E_1, E_3, and E_5. This separation is essential for a clear differentiation between cells susceptible to COVID-19 and those susceptible to MRSA infection.

2.3. **Coupling Mechanism Between the Between-Host and Within-Host Dynamics.** The multiscale model presented here consists of two interconnected components: the between-host model (see Equations 2.9-2.16) and the within-host model (see Equations 2.32-2.46). These components are linked through several transmission rates: $\beta_1(V_1)$, $\beta_2(B_1)$, $\beta_3(V_2, B_2)$, $\beta_4(B_1)$ and $\beta_5(V_1)$, as described in Equations (2.9), (2.10), (2.11), and (2.12). These transmission rates are influenced by the quantities of virus and bacteria present in the body. Also, the contribution rates of SARS-CoV-2 and bacteria from the environment into the human host are denoted as f_1, f_2, f_3 and f_4, as shown in Equations (2.34), (2.38), (2.43), and (2.44). In essence, higher levels of viral and bacterial load in human hosts can lead to increased transmission rates, while higher levels of viral and bacterial load in the physical environment can result in higher contribution rates to the in-host virus and bacteria [82], [50]. Thus, the complete multiscale model is as follows:

$$\begin{aligned}\frac{dS_H}{dt} &= \Lambda - \beta_1(V_1)S_H I_C - \alpha_1\beta_1(V_2)S_H I_{CM} - \beta_2(B_1+B_M)S_H I_M - \alpha_2\beta_2(B_2+B_N)S_H I_{CM} - \\ &\quad (1-\alpha_1)(1-\alpha_2)\beta_3(V_2, B_2+B_N)S_H I_{CM} - \alpha_3 S_H V_E - \mu S_H, \qquad (2.47)\\ \frac{dI_C}{dt} &= \beta_1(V_1)S_H I_C + \alpha_1\beta_1(V_2)S_H I_{CM} + \alpha_3 S_H V_E - \beta_4(B_1+B_M)I_C I_M \\ &\quad -(\nu + a + \delta_1 + \mu)I_C, \qquad (2.48)\end{aligned}$$

$$\frac{dI_M}{dt} = \beta_2(B_1+B_M)S_H I_M + \alpha_2\beta_2(B_2+B_N)S_H I_{CM} - \beta_5(V_1)I_M I_C - \beta_6 I_M V_E - (r+b+\delta_2+\mu)I_M, \tag{2.49}$$

$$\frac{dI_{CM}}{dt} = (1-\alpha_1)(1-\alpha_2)\beta_3(V_2,B_2+B_N)S_H I_{CM} + \beta_4(B_1+B_M)I_C I_M + \beta_5(V_1)I_M I_C + \beta_6 I_M V_E - (\omega+l+\delta_3+\mu)I_{CM}, \tag{2.50}$$

$$\frac{dJ}{dt} = aI_C + bI_M + lI_{CM} - (n+\delta_4+\mu)J, \tag{2.51}$$

$$\frac{dV_E}{dt} = p_1 I_C + p_2\tau_1 I_{CM} - h_1 V_E, \tag{2.52}$$

$$\frac{dB_E}{dt} = \lambda_1 I_M + \lambda_2\tau_2 I_{CM} - h_2 B_E, \tag{2.53}$$

$$\frac{dR}{dt} = \nu I_C + rI_M + \omega I_{CM} + nJ - \mu R, \tag{2.54}$$

$$\frac{dE_1}{dt} = \varepsilon_1 - \psi_1 E_1 V_1 - \rho_1 E_1, \tag{2.55}$$

$$\frac{dE_2}{dt} = \psi_1 E_1 V_1 - \rho_1 E_2, \tag{2.56}$$

$$\frac{dV_1}{dt} = f_1 V_E + \kappa_1 E_2 - e_1 N_1 V_1 - \rho_2 V_1, \tag{2.57}$$

$$\frac{dN_1}{dt} = \pi_1 + \sigma_1 N_1 E_2 - \phi_1 N_1, \tag{2.58}$$

$$\frac{dE_3}{dt} = \varepsilon_2 - \psi_2 E_3(B_1+B_M) - \varphi E_3, \tag{2.59}$$

$$\frac{dE_4}{dt} = \psi_2 E_3(B_1+B_M) - \varphi E_4, \tag{2.60}$$

$$\frac{dB_1}{dt} = f_2 B_E + (1-\theta)\gamma_1 B_1\left(1-\frac{B_1+B_M}{K_1}\right) - e_2 N_2 B_1 - sB_1 m - d_1 B_1, \tag{2.61}$$

$$\frac{dB_M}{dt} = (1-\theta)\gamma_1 B_M\left(1-\frac{B_1+B_M}{K_1}\right) + sB_1 m - e_3 N_2 B_M - d_1 B_M, \tag{2.62}$$

$$\frac{dN_2}{dt} = \pi_2 + \sigma_2 N_2 E_4 - \phi_2 N_2, \tag{2.63}$$

$$\frac{dE_5}{dt} = \varepsilon_3 - \psi_3 E_5(B_2+B_N) - \psi_4 E_5 V_2 - \zeta E_5, \tag{2.64}$$

$$\frac{dE_6}{dt} = \psi_3 E_5(B_2+B_N) + \psi_4 E_5 V_2 - \zeta E_6, \tag{2.65}$$

$$\frac{dV_2}{dt} = f_3 V_E + \kappa_2 E_6 - z_1 N_3 V_2 - \rho_3 V_2, \tag{2.66}$$

$$\frac{dB_2}{dt} = f_4 B_E + (1-\theta)\gamma_2 B_2\left(1-\frac{B_2+B_N}{K_2}\right) - z_2 N_3 B_2 - uB_2 m - d_2 B_2, \tag{2.67}$$

$$\frac{dB_N}{dt} = (1-\theta)\gamma_2 B_N\left(1-\frac{B_2+B_N}{K_2}\right) + uB_2 m - z_3 N_3 B_N - d_2 B_N, \tag{2.68}$$

$$\frac{dN_3}{dt} = \pi_3 + \sigma_3 N_3 E_6 - \phi_3 N_3. \tag{2.69}$$

Remark 2.3.1. In our co-infection model, we have included the population dynamics of neutrophils (N_1, N_2, N_3) within the within-host scale due to their pivotal role in the innate immune response against bacterial and viral infections (e.g., SARS-CoV-2) [54], as detailed in Equations (2.58), (2.63), and (2.69). We focus on the innate immune response to viruses, which come into action within hours following viral

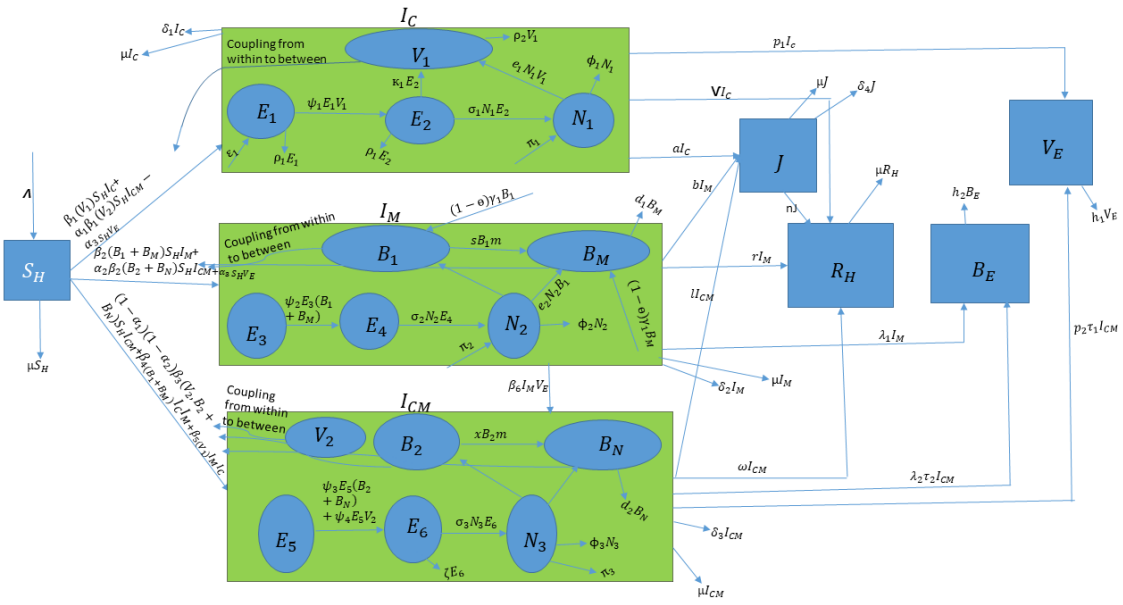

FIGURE 1. Linked Within-host and Between-host Transmission Diagram of COVID-19-MRSA Coinfection

infection. Although the model does not explicitly encompass equations for other immune cell types or immune response molecules, this simplification is reasonable, given the complexity inherent in modeling the entire immune response within a multiscale framework. Focusing on neutrophils as representatives of the innate immune response is justified, particularly when investigating co-infection dynamics, and aligns with the research objectives of exploring the impact of immunomodulatory antibiotics, such as azithromycin, which enhances immune cell function, including that of neutrophils.

For a visual description of the transmission dynamics of the multiscale model, please see the diagram in Figure 1.

Motivated by Wang et al [88], the functions $\beta_1(V_1)$, $\beta_2(B_1)$, $\beta_3(V_2, B_2)$, $\beta_4(B_1)$ and $\beta_5(V_1)$ describing how the viral load inside an infected individual (within-host) leads to viral and bacterial transmission between-hosts are defined as:

$$\beta_1(V_1) = \beta_1^0 + q_0 V_1, \tag{2.70}$$

$$\beta_2(B_1) = \beta_2^0 + q_0 B_1, \tag{2.71}$$

$$\beta_3(V_2, B_2) = \beta_3^0 + q_0 V_2 + q_0 B_2, \tag{2.72}$$

$$\beta_4(B_1) = \beta_4^0 + g_0 B_1, \tag{2.73}$$

$$\beta_5(V_1) = \beta_5^0 + g_0 V_1. \tag{2.74}$$

where baseline transmission rates (β_1^0, β_2^0, β_3^0, β_4^0, and β_5^0) represent the transmission rates when the viral and bacterial load are extremely low and not detectable by the Reverse Transcription Polymerase Chain Reaction known as RT-PCR which is used for SARS-CoV-2 detection [11] and Polymerase Chain

TABLE 2. Description of state variables of MRSA and COVID-19 co-infection model

Variables	Decription
S_H	Susceptible individuals to COVID-19 and MRSA
I_C	Individuals infected with COVID-19
I_M	Individuals infected with MRSA
I_{CM}	Individuals co-infected with COVID-19 and MRSA
J	Isolated individuals
V_E	Environmental virus
B_E	Environmental MRSA
R	Recovered individuals
E_1	Uninfected cells in I_C
E_2	Infected cells with COVID-19 in I_C
V_1	Within-host SARS-CoV-2 in I_C
N_1	Population of Neutrophils in I_C
E_3	Uninfected cells in I_M
E_4	Infected cells with MRSA in I_M
B_1	Population of MSSA in I_M
B_M	Population of MRSA in I_M
N_2	Population of Neutrophils in I_M
E_5	Uninfected cells with COVID-19 and MRSA
E_6	Co-infected cells with COVID-19 and MRSA
V_2	Within-host SARS-CoV-2 in I_{CM}
B_2	Population of MSSA in I_{CM}
B_N	Population of MRSA in I_{CM}
N_3	Population of Neutrophils in I_{CM}

Reaction, known as PCR which is used for MRSA detection [45],[43] (RT-PCR targets viral RNA, while PCR targets MRSA DNA, reflecting the difference in genetic material between a virus and a bacterium). This scenario corresponds to individuals who have recently contracted COVID-19 and MRSA bacteria, but the pathogens (virus and MRSA) have not yet reached detectable levels through RT-PCR [51], and PCR [55]. However, even at this early stage, some transmission can still occur, although at a low level [76]. In the multiscale model, the within-host virus and bacteria populations correspond to the populations of virus and bacteria detected by RT-PCR and PCR within a host. The parameters q_0 and g_0 determine how the detected viral and bacterial load measured by RT-PCR influence the transmission rates, thus reflecting the impact of the viral and bacterial load on transmission rates. When $V_1 = 0$, $B_1 = 0$, $V_2 = 0$, and $B_2 = 0$, the transmission rates solely depend on the baseline transmission rates (β_1^0, β_2^0, β_3^0, β_4^0, and β_5^0) associated with very low viral and bacterial load (below the clinical detection threshold). Conversely, when $V_1 \neq 0$, $B_1 \neq 0$, $V_2 \neq 0$, $B_2 \neq 0$, the transmission rates increase. This highlights the influence of the viral and bacterial load on the contagiousness of the disease, with higher levels of viral and bacterial load contributing more significantly to the overall transmission rates.

The initial conditions for the multiscale model are given below:

$$
\begin{aligned}
&S_H(0) = S_H^0 \geq 0,\ I_C(0) = I_C^0 \geq 0,\ I_M(0) = I_M^0 \geq 0,\ I_{CM}(0) = I_{CM}^0 \geq 0,\ J(0) = J^0 \geq 0,\\
&V_E(0) = V_E^0 \geq 0,\ B_E(0) = B_E^0 \geq 0,\ R(0) = R^0 \geq 0, E_1(0) = E_1^0 \geq 0,\ E_2(0) = E_2^0 \geq 0,\\
&V_1(0) = V_1^0 \geq 0,\ N_1(0) = N_1^0 \geq 0,\ E_3(0) = E_3^0 \geq 0,\ E_4(0) = E_4^0 \geq 0,\ B_1(0) = B_1^0 \geq 0,\\
&B_M(0) = B_M^0 \geq 0,\ N_2(0) = N_2^0 \geq 0,\ E_5(0) = E_5^0 \geq 0,\ E_6(0) = E_6^0 \geq 0,\ V_2(0) = V_2^0 \geq 0,\\
&B_2(0) = B_2^0 \geq 0,\ B_N 2(0) = B_N^0 \geq 0,\ N_3(0) = N_3^0 \geq 0.
\end{aligned}
$$

Remark 2.3.2. The key difference in dynamics between these two scales lies in their focus and level of detail. The between-host scale looks at how infections spread and interact at the population level, while the within-host scale explores the detailed processes occurring within an individual's body. The interactions, transmission, and immune responses are described differently at each scale to capture the relevant aspects of the disease's progression.

3. Results

3.1. **Disease-Free Equilibrium and Basic Reproduction Number.** The system (2.47)-(2.69) has a disease-free equilibrium given by

$$\begin{aligned} E_0 &= (S_H, I_C, I_M, I_{CM}, J, V_E, B_E, R, E_1, E_2, V_1, N_1, E_3, E_4, B_1, B_M, N_2, E_5, E_6, V_2, B_2, B_N, N_3), \\ &= \left(\frac{\Lambda}{\mu}, 0, 0, 0, 0, 0, 0, 0, \frac{\varepsilon_1}{\rho_1}, 0, 0, \frac{\pi_1}{\phi_1}, \frac{\varepsilon_2}{\varphi}, 0, 0, 0, \frac{\pi_2}{\phi_2}, \frac{\varepsilon_3}{\zeta}, 0, 0, 0, 0, \frac{\pi_3}{\phi_3}\right). \end{aligned}$$

Using the next generation operator of [21], the basic reproduction number is calculated as

$$R_0 = \vartheta(FG^{-1}) = \max\{R_B, R_W\},$$

where

$$R_B = \frac{\beta_2\Lambda}{\mu(r+b+\delta_2+\mu)} + \frac{\Lambda(\alpha_3 p_1 + \beta_1 h_1)}{\mu h_1(\nu+a+\delta_1+\mu)} + \frac{\Lambda\beta_3(1-\alpha_1)(1-\alpha_2)}{\mu(\omega+l+\delta_3+\mu)}$$

and

$$R_W = \frac{\psi_1\varepsilon_1\kappa_1\phi_1}{\rho_1^2(\pi_1 e_1+\rho_2\phi_1)} + \frac{(1-\theta)\gamma_1\phi_2}{d_1\phi_2+e_3\pi_2} + \frac{(1-\theta)\gamma_1\phi_2}{ms\phi_2+d_1\phi_2+e_2\pi_2} + \frac{\psi_4\varepsilon_3\kappa_2}{\zeta^2\rho_3} + \frac{(1-\theta)\gamma_2\phi_3}{d_2\phi_3+\pi_3 z_3} + \frac{(1-\theta)\gamma_2\phi_3}{\mu\phi_3+d_2\phi_3+\pi_3 z_2}.$$

R_B refers to the average number of secondary infections caused by an infected person in a completely susceptible population during their infectious period, while R_W refers to the average number of secondary infections caused by a productive epithelial cell in a virus-free and bacteria-free epithelial cell population. The maximum value of R_B and R_W is the basic reproduction number R_0.

4. Parameter Estimation and Global Sensitivity Analysis

4.1. **Parameter Estimation.** Parameter estimation plays a crucial role in fitting mathematical models to real-world data, as it allows for the estimation of model parameters that cannot be directly measured. Therefore, this section of the study involves estimating the parameters in model $(2.47) - (2.69)$ using real data of COVID-19 infected cases in France [20]. The COVID-19 confirmed cases data from August 7 to October 22, 2022, was considered for the analysis. The European Centre for Disease Prevention and Control (ECDC) is a reputable and reliable source for epidemiological data related to infectious diseases, including COVID-19 [27]. The dataset provided by the ECDC offers comprehensive coverage of multiple EU/EEA countries, ensuring a wide range of data points for analysis. Before fitting the data to the model, certain information related to the parameters was determined. For instance, the natural death rate of individuals was calculated by taking the reciprocal of the average life expectancy (in days) of the French population in 2022, which was 83 years [28]. The total population of France in 2022 was estimated to be approximately $67,900,000$ [86], and the recruitment rate of susceptible individuals was obtained from the total population and the natural death rate. We performed a simulation using the fmincon package in MATLAB. Our code utilized the Least Square Method to solve the nonlinear data fitting problem. Specifically, we input the observed output data (y_{data}) and corresponding input data (t_{data}), and determined the coefficients that provides the best fit for the equation

$$\min_x \|F(x, t_{\text{data}}) - y_{\text{data}}\|_2^2 = \min_x \sum_i \left(\left(F(x, t_{\text{data}_i}) - y_{\text{data}_i}\right)\right)^2.$$

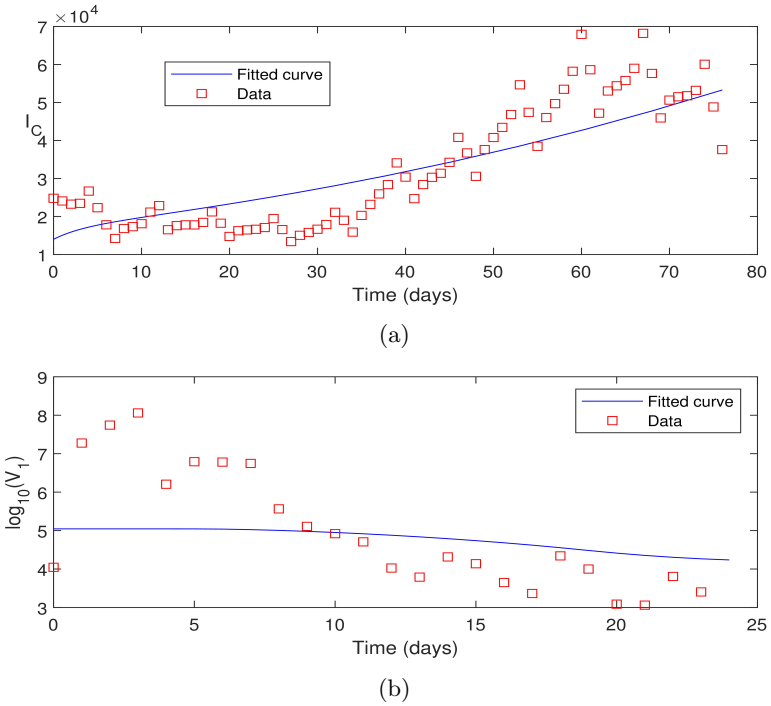

FIGURE 2. Model fitting to match the average viral load data observed in Germany [84] (see Figure 2(b)) and the number of COVID-19 cases in France from 7 August to 22 October, 2022 [20] (see Figure 2(a))

For the immunological part of the multiscale model, the SARS-CoV-2 viral load data was fitted to the model using nonlinear square method. Daily measurements of viral load in sputum, pharyngeal swabs, and stool for nine patients in Germany, were reported in [84], and the model was fitted to both viral load and confirmed cases data simultaneously. The other parameter values were chosen from the well-established literature or assumed, as the available data in [20],[84], was not sufficient to estimate all the parameters involved in the dynamics of the disease. The solution curve for individuals infected with COVID-19 (denoted as I_C) was fitted to the "active cases" data (see Figure 2(a)), while the solution curve for within-host SARS-CoV-2 in I_C (denoted as V_1) was fitted to the "average viral load" data (see Figure (2b)) and the best fit were displayed in Figures 2(a) and 2(b). Table 1 provides a summary of the calculated and predicted parameters, which have been sourced from both our model fitting and parameter estimation process, as well as from previous literature. Based on the parameter values listed in Table 1, the estimated between-host and within-host reproduction numbers, denoted as R_B and R_W respectively, were determined to be 3.8008 and 6.9382. After parameter estimation, sensitivity analysis is carried out to test the sensitivity of the model to different parameter values, which can help identify which parameters have the most significant influence on the model's behaviour.

Remark 4.1.1. The disparities observed in Figure 2, depicting the trajectory of within-host SARS-CoV-2 (V_1) between model simulations and empirical data, can be attributed to several factors. Firstly, the model's fitting process solely considered viral load data and did not account for bacterial dynamics, despite the model incorporating equations for both viruses and bacteria. This omission could lead to inconsistencies, as viral and bacterial interactions can influence each other's dynamics. Additionally,

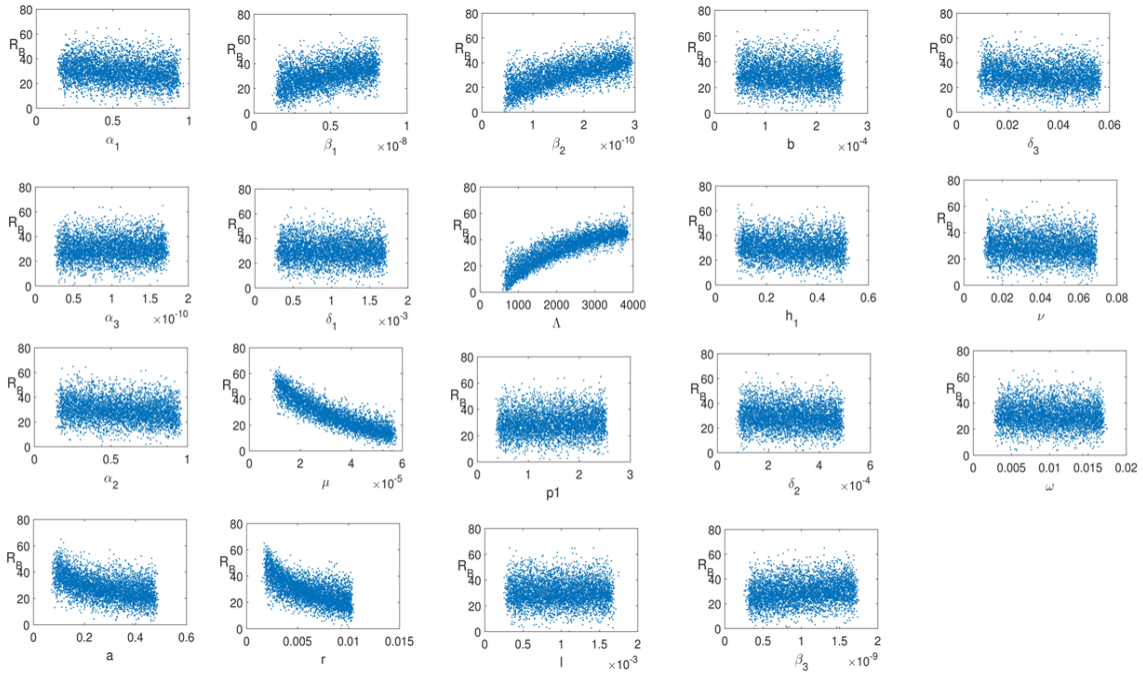

(A) Scatter plots for between-host

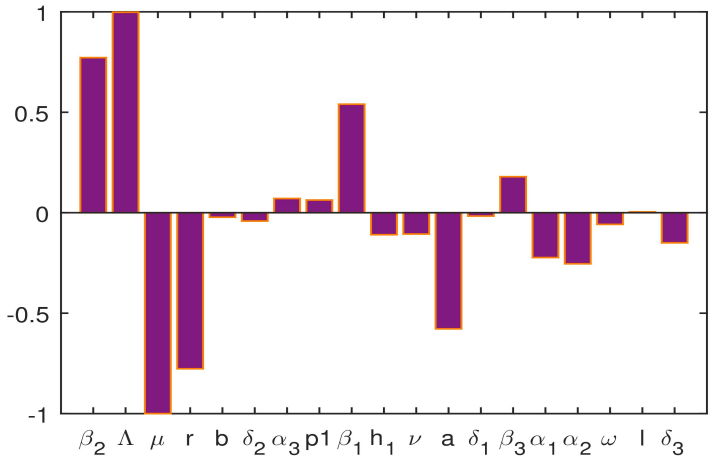

(B) PRCC bar chart for between-host

FIGURE 3. Sensitivity analysis for between-host

the quality and quantity of available data, as well as inherent biological variability, play a role in these disparities. The interactions between within-host SARS-CoV-2 and bacteria, as well as their impact on between-host dynamics, introduce complexities that may require more comprehensive data.

4.2. **Global Sensitivity Analysis.** Global sensitivity analysis of the between-host and within-host reproduction numbers are carried out in this section. It is a statistical method which involves analyzing

the model output as a function of all input parameters simultaneously, as opposed to local sensitivity analysis, which focuses on the effect of changing one parameter at a time. It can help identify which parameters have the greatest impact on the spread of the virus both within and between individuals. The model includes several parameters that are uncertain or assumed, and the global sensitivity analysis allows for the quantification of the impact of each parameter on the model output. By using Latin Square Sampling and Partial Rank Correlation Coefficient (PRCC) methods [83], global sensitivity analysis can identify the parameters with the most significant impact on the between-host and within-host reproduction numbers.

4.2.1. *Global Sensitivity Analysis of R_B.* We perform a global sensitivity analysis on an epidemiological part of the multiscale model that contains several parameters. The analysis used Latin Square Sampling and Partial Rank Correlation Coefficient (PRCC) methods [71] and a sample size of 5000. Figures (3a) and (3b) show PRCCs values of parameters against R_B. The parameters are varied simultaneously over a specified range with each parameter being set to 75% below and 75% above its baseline value, to assess their impact on the model's output. The results obtained from the analysis show that some parameters have a significant impact on the between-host reproduction number (R_B), which is a key metric in the model. Firstly, it is evident that the recruitment rate of humans Λ and the infection rate of MRSA (β_2) are the most influential parameters positively affecting the between-host reproduction number (R_B). This implies that strategies to reduce MRSA transmission and increase the recruitment of new individuals into the population can have a substantial impact on the overall spread of COVID-19 and MRSA co-infection. Additionally, the infection rate of COVID-19 (β_1) and the co-infection rate of COVID-19 and MRSA also positively contribute to R_B, highlighting the importance of controlling the spread of both infections simultaneously. Conversely, certain parameters have a large negative impact on R_B, indicating their significance in mitigating the spread of co-infections. These parameters include the natural mortality rate (μ), the recovery rate of individuals infected with MRSA (r), and the isolation rate of individuals infected with COVID-19 (a). These findings emphasize the critical role of healthcare interventions, recovery strategies, and mortality reduction in limiting the transmission of COVID-19 and MRSA co-infection. Furthermore, parameters with smaller negative impacts on R_B include the fraction of susceptible individuals (S_H) who have contact with co-infected individuals but are only infected with COVID-19 (α_2) and the fraction infected with MRSA only (α_1), along with the disease-induced death rate of co-infected individuals (δ_3). These results underscore the importance of identifying individuals with specific infections and tailoring interventions accordingly to reduce transmission. Thus, effective strategies to control these infections should prioritize interventions that target recruitment rates, infection rates, recovery rates, mortality reduction, and the identification of specific infection cases. These findings provide valuable insights for policymakers and healthcare professionals in managing and mitigating the impact of co-infections, ultimately leading to improved public health outcomes.

4.2.2. *Global Sensitivity Analysis of R_W.* A global sensitivity analysis was conducted to assess the impact of various model parameters on the within-host reproduction number (R_W) of COVID-19 and MRSA coinfection, and two key scenarios were considered: when methicillin (m) is absent ($m = 0$) and when methicillin is present ($m = 1$). The analysis employed the Latin Hypercube Sampling Method, generating a sample size of 5000, and measured the sensitivity of R_W to parameter variations. Figure 4 shows scatter plots of parameters against R_W when $m = 0$ (Subfigure 4(a)) and PRCCs values of parameters against R_W for both $m = 0$ and $m = 1$ (Subfigure 4(b)). Among the key parameters that positively affect R_W in Subfigure (4b), five stand out: The intrinsic growth rate of staphylococcus aureus in individuals infected with MRSA (γ_1), the intrinsic growth rate of staphylococcus aureus in

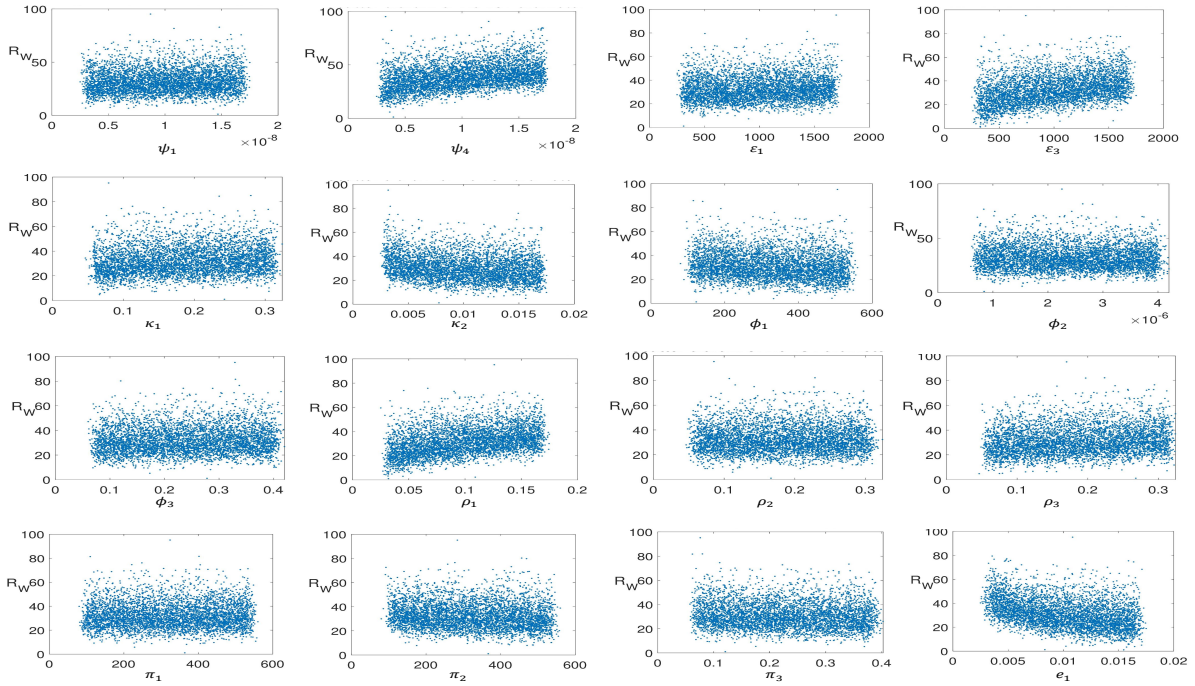

(A)

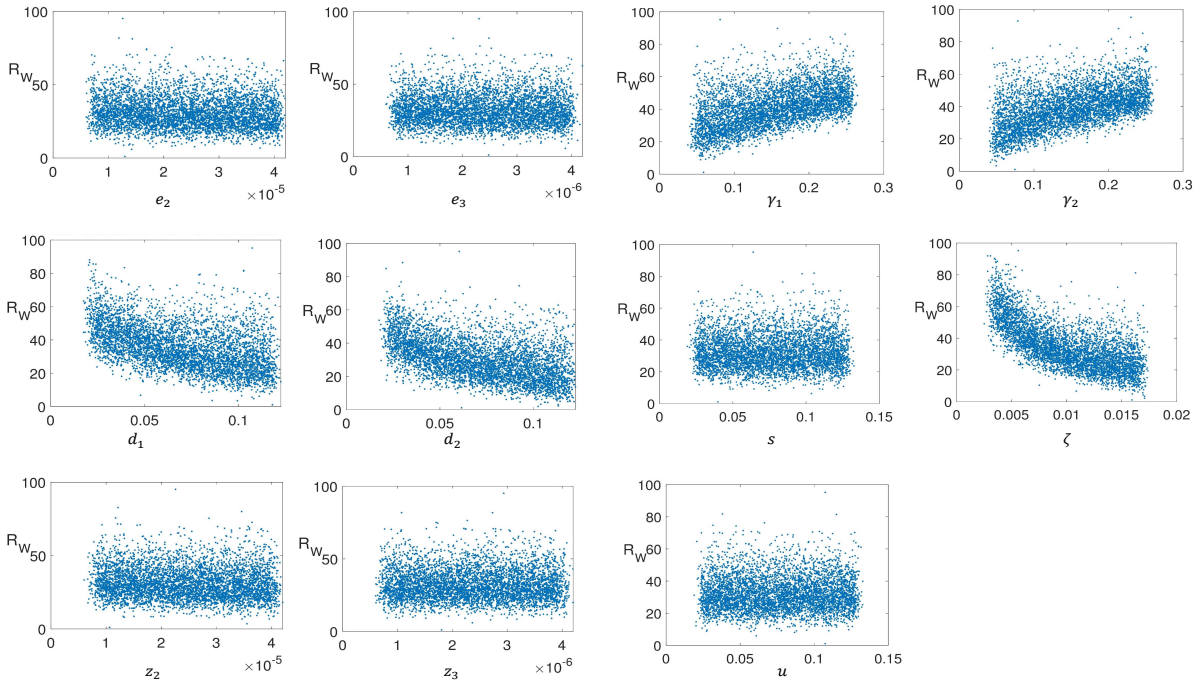

(B)

4(a): Scatter plots for within-host when $m = 0$

individuals coinfected with COVID-19 and MRSA (γ_2), the production rate of virus from coinfected cells

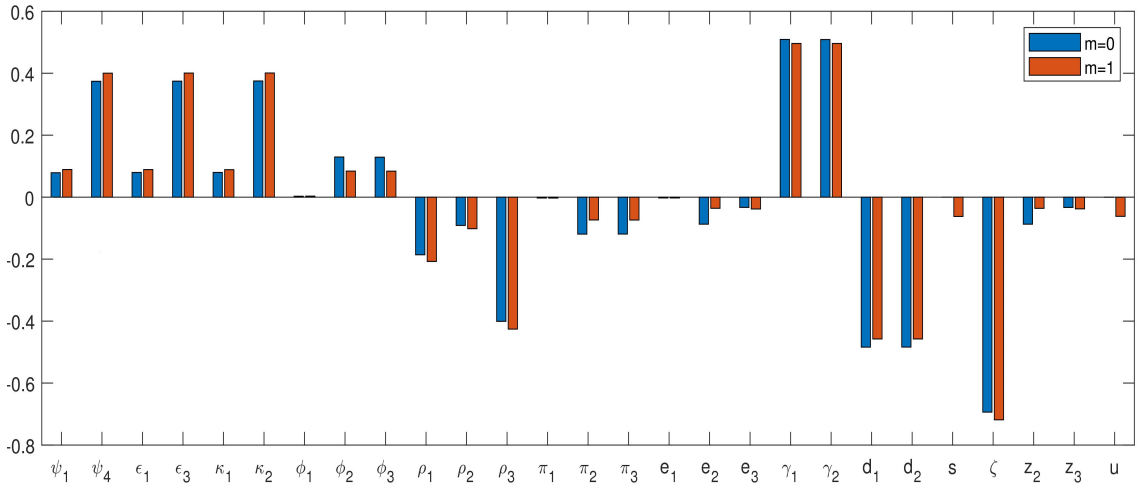

FIGURE 5. PRCC bar chart for within-host when $m = 0$ and $m = 1$

in individuals coinfected with COVID-19 and MRSA (κ_2), the constant regeneration rate of COVID-19-MRSA uninfected cells (ε_3), and the infection rate of COVID-19-MRSA uninfected cells by SARS-CoV-2 (ψ_4). When methicillin is present ($m = 1$), γ_1 and γ_2 exhibit a substantial positive impact on R_W. However, in the absence of methicillin ($m = 0$), these parameters (γ_1 and γ_2), have an even more pronounced positive effect. Further, κ_2, ε_3, and ψ_4 contribute positively to R_W in both scenarios (when $m = 0$ and $m = 1$), and κ_2, ε_3 and ψ_4 have an even more substantial positive effect in the presence of methicillin (when $m = 1$). Conversely, the parameters ζ, d_1, d_2, ρ_3, and ρ_1 exert negative effects on R_W. When methicillin is not used ($m = 0$), ζ, representing the natural death rate of COVID-19-MRSA uninfected cells in compartment I_{CM}, has a large negative impact on R_W, which becomes even more substantial when methicillin is introduced ($m = 1$). Similarly, d_1 and d_2, which denote the decay rates of MRSA bacteria in compartments I_M and I_{CM} respectively, have significant negative effects on R_W, with d_1 and d_2 having a greater impact when methicillin is not used. Furthermore, ρ_3 and ρ_1, representing the death rates of V_2 in I_{CM} and COVID-19 uninfected cells inside I_C, respectively, exhibit large negative effects on R_W, which become even more pronounced when methicillin is introduced ($m = 1$). These results highlight the importance of understanding how methicillin usage can modulate the impact of various parameters on R_W and emphasize the need for careful consideration when managing COVID-19 and MRSA coinfection in the context of antibiotic resistance and alternative treatment strategies.

Therefore, based on the findings, several targeted strategies can be implemented. Firstly, when methicillin is used ($m = 1$), efforts should focus on lowering the intrinsic growth rates of staphylococcus aureus (γ_1 and γ_2) through appropriate antibiotic regimens and infection control measures. Additionally, boosting the effectiveness of methicillin or alternative antibiotics to further suppress bacterial growth is vital. In the absence of methicillin ($m = 0$), similar strategies to reduce the intrinsic growth rates of MRSA are crucial. Further, focusing on increasing the natural death rate of COVID-19-MRSA uninfected cells in compartment I_{CM} (ζ) and the decay rates of MRSA bacteria in compartments I_M and I_{CM} (d_1 and d_2) can further contribute to lowering R_W, especially when methicillin is not used. Moreover, increasing the death rate of virus within I_C can be achieved by administering drugs that can induce apoptosis (programmed cell death) of infected cells or inhibit the replication of the virus [39]. The effectiveness of antiviral drugs such as remdesivir and molnupiravir in targeting and controlling viral infections like COVID-19, rely on the proper functioning of the immune response. However, if

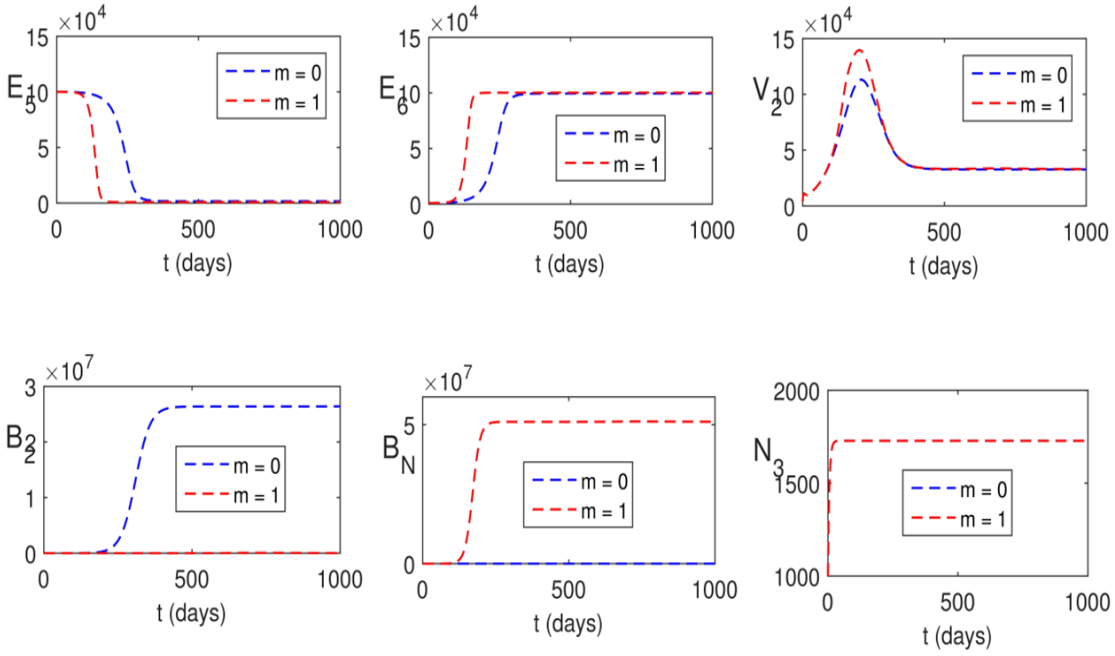

FIGURE 6. Simulations of the dynamics of COVID-19 and MRSA co-infection within the host without and with methicillin ($m = 0$ and $m = 1$) in the absence of vancomycin and immunomodulatory antibiotics

the immune response is disrupted due to the use of antibiotics like methicillin, nafcillin, cefazolin, and dicloxacillin, which are typically used to treat bacterial infections including staphylococcus aureus, it can potentially undermine the effectiveness of these antiviral treatments. This disruption of the immune response can have implications on the dynamics of the coinfection, including the severity of symptoms, the progression of the diseases, and the overall outcome. Therefore, it is essential to understand the specific impact of methicillin on the dynamics of the coinfection.

5. Numerical Simulations

In this section, we analyze the dynamics of the multiscale model (2.47)-(2.69) in the presence of methicillin (m=1) using numerical simulations. Our primary objectives are to understand the impact of methicillin on the dynamics of coinfection and evaluate the effectiveness of immunomodulatory antibiotics and vancomycin in reducing MRSA bacterial infections. We provide discussion of the numerical results obtained from the simulations in what follows.

Figures 5 and 6 show the time evolution of within-host dynamics in individuals coinfected with COVID-19 and MRSA (I_{CM}) as well as individuals singly infected with MRSA (I_M), after methicillin treatment, when vancomycin and immunomodulatory antibiotics have not been administered. In individuals coinfected with COVID-19 and MRSA (I_{CM}), methicillin treatment ($m = 1$) increases populations of co-infected cells (E_6), SARS-CoV-2 virus (V_2), and MRSA bacteria (B_N) but decreases methicillin-sensitive Staphylococcus aureus (B_2) (see Figures 5 and 6). Neutrophil populations (N_3) remain stable, unaffected by methicillin presence in Figure 5, but in Figure 6, neutrophil populations

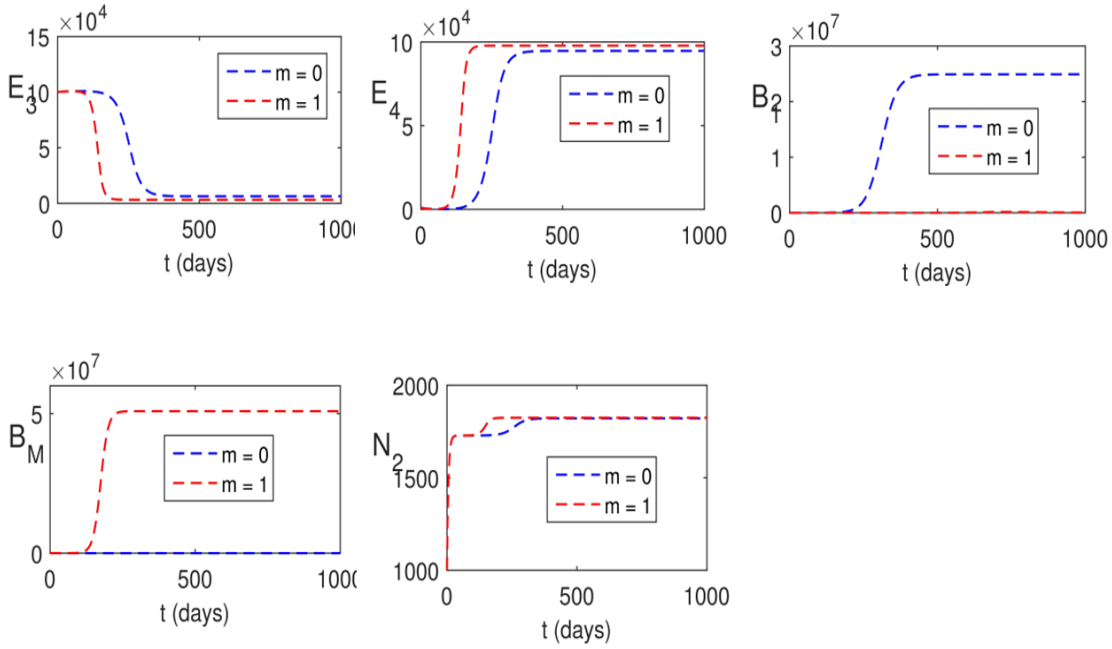

FIGURE 7. Simulations of the dynamics of MRSA only within the host without and with methicillin ($m = 0$ and $m = 1$) in the absence of vancomycin and immunomodulatory antibiotics

in I_M (N_2) exhibit a slight increase with methicillin and a minor decrease without it. Additionally, Figure 7 shows that in COVID-19-infected individuals (I_C), viral load (V_1), and infected cells (E_2), cases $m = 0$ and $m = 1$ exhibit no differences. These findings indicate that methicillin's impact is more significant on bacterial populations than on the immune response, potentially leading to an increase in methicillin-resistant staphylococcus aureus (MRSA) due to selective pressure from the antibiotic [17], while methicillin-sensitive strains may decline in the presence of the drug. Furthermore, Figure 8 demonstrates that methicillin does not alter populations of individuals infected with COVID-19 (I_C) or environmental virus (V_E), but a slight increase is observed in populations of individuals infected with MRSA (I_M), co-infected individuals (I_{CM}), environmental MRSA bacteria (B_E), and isolated individuals (J) when methicillin is used ($m = 1$). Therefore, using methicillin treatment in co-infected individuals may lead to an increase in the prevalence of drug-resistant bacteria, which can be a concern in managing infectious diseases. Hence, it may be useful to explore alternative treatment options or combination therapies to avoid the development of drug resistance.

Thus, we further assess vancomycin antibiotics' impact on MRSA and COVID-19-MRSA coinfected cells at varying effectiveness levels in the presence of methicillin and without immunomodulatory antibiotics. Figure 9 shows that increasing vancomycin effectiveness from 50% to 90% reduces MRSA populations in I_M (B_M) and I_{CM} (B_N), with no change in other cell populations. Figure 10 simulates the within-host coinfection dynamics of COVID-19 and MRSA with different levels of immunomodulatory antibiotics (azithromycin) on in-host coinfected cells, in the absence of vancomycin and presence

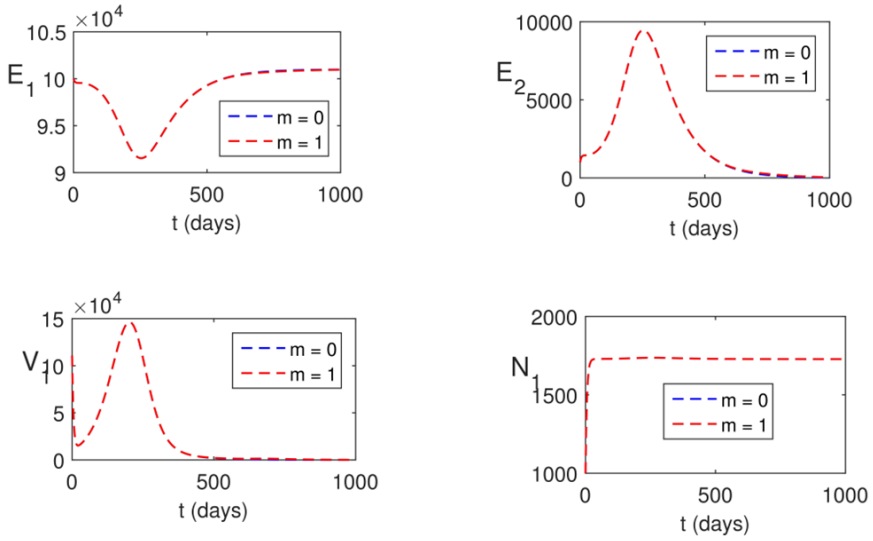

FIGURE 8. Simulations of the dynamics of COVID-19 only within the host without and with methicillin ($m = 0$ and $m = 1$) in the absence of vancomycin and immunomodulatory antibiotics

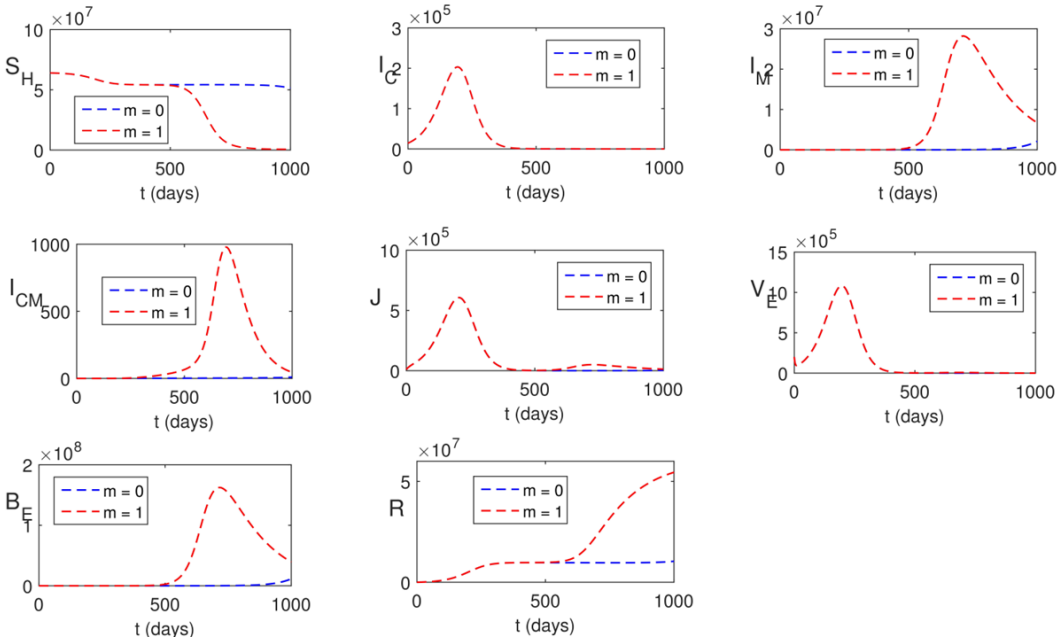

FIGURE 9. Simulations of the dynamics of between-host population without and with methicillin ($m = 0$ and $m = 1$) in the absence of vancomycin and immunomodulatory antibiotics

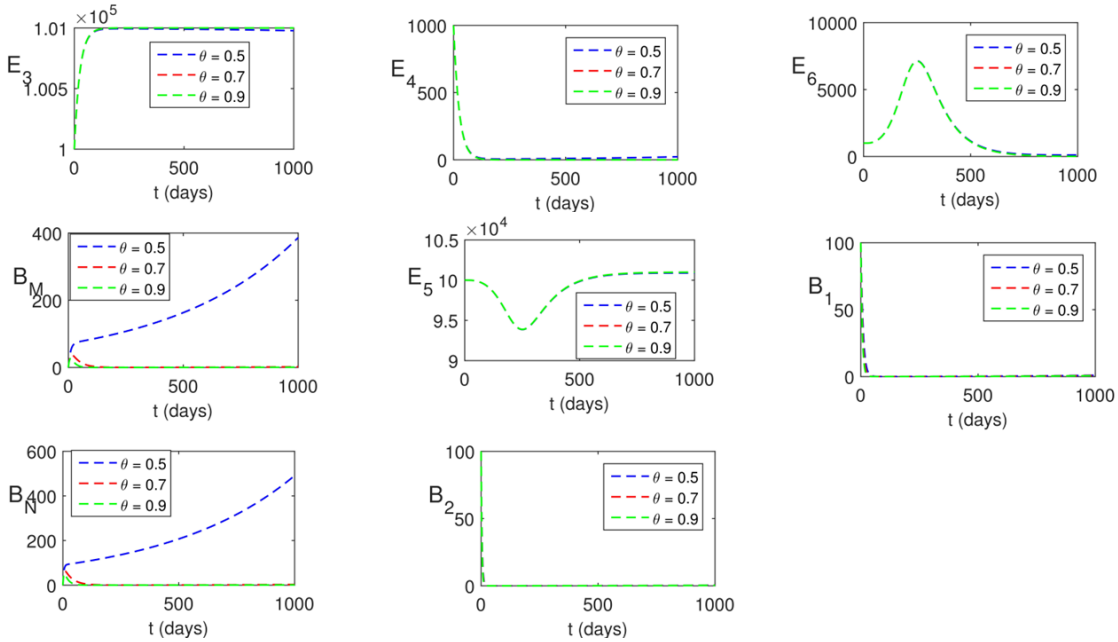

FIGURE 10. Simulations showing the dynamics of the MRSA infected cells and COVID-MRSA coinfected cells under different levels of vancomycin in the absence of immunomodulatory antibiotics with $m = 1$

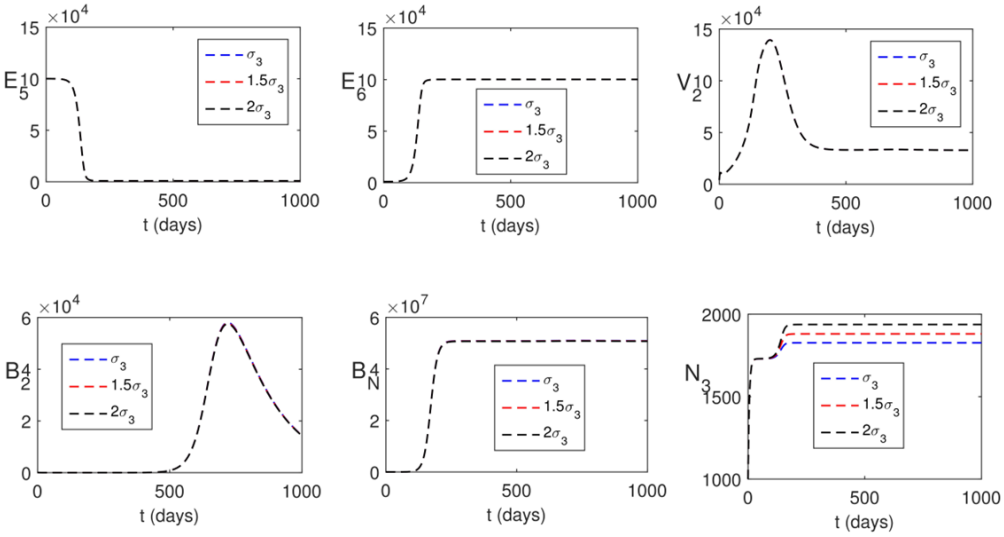

FIGURE 11. Dynamics of the in-host model under different levels of immunomodulatory antibiotics within individuals co-infected with COVID-19 and MRSA in the absence of vancomycin with $m = 1$

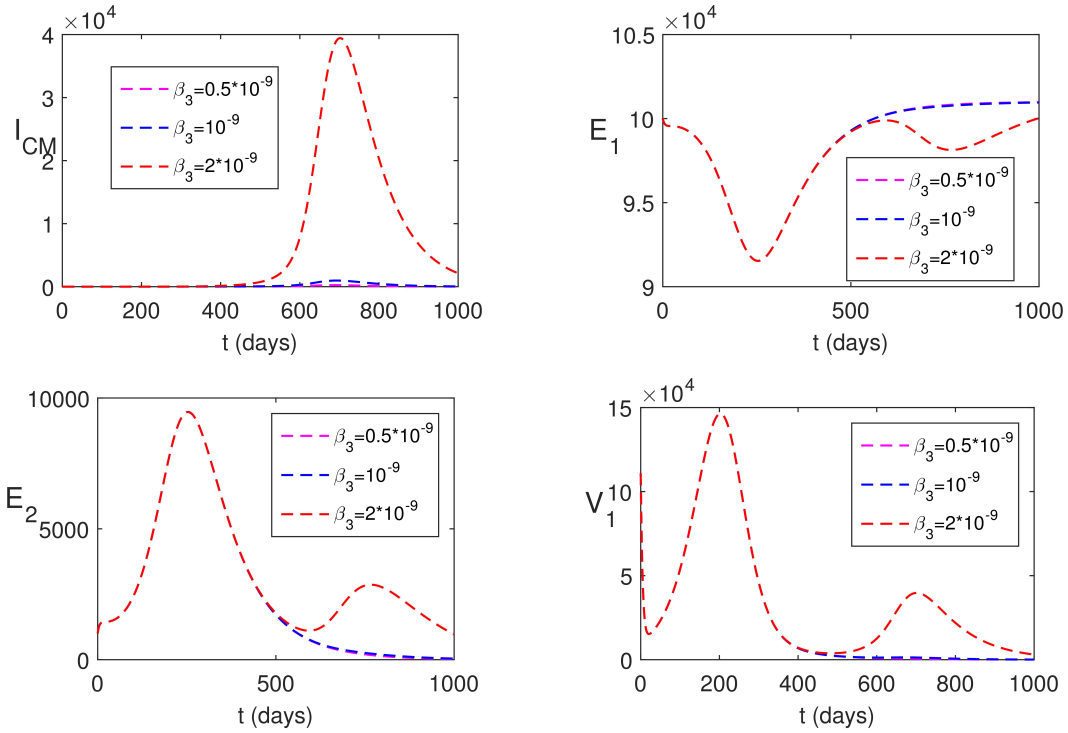

FIGURE 12. The dynamics of the multiscale model for different values of co-infection rate of COVID-19 and MRSA denoted as β_3 given in the legend, and other parameter values are given in Table 1

of methicillin. The numerical results indicate that increasing the efficacy of immunomodulatory antibiotics (σ_3) leads to an increase in the population of neutrophils (N_3) only, and does not have impacts on other cells.

5.1. **Impact of Coinfection Rate on the Dynamics.** In this section, we present and discuss the outcomes of varying the coinfection rate of COVID-19 and MRSA (β_3) within the multiscale model and its consequential impact. Figure 11 visually represents these effects, and the following observations were made: Firstly, at the between-host scale, an increase in individuals coinfected with COVID-19 and MRSA (I_{CM}) was observed with higher β_3 values, while no effect of β_3 was detected on other populations at the between-host scale. At the within-host scale, the population of infected cells with COVID-19 in I_C (E_2) increased significantly with higher β_3 values, and it decreased with lower values of β_3. Additionally, the within-host SARS-CoV-2 in individuals infected with COVID-19 (V_1), showed a minor increase with higher β_3 values, while no impact of β_3 was identified on other cell populations within the within-host scale.

6. CONCLUSION

This study focused on the multiscale modeling of the transmission dynamics of COVID-19 and MRSA coinfection in the hospital, incorporating the effects of traditional antibiotics (methicillin and vancomycin) and immunomodulatory antibiotics (azithromycin) on the dynamics of the coinfection. Vancomycin and methicillin antibiotics were investigated because of their clinical relevance. Vancomycin are widely prescribed antibiotics for treating MRSA infections, including cases of coinfection with other

TABLE 3. Summary of findings

Findings	**Interpretation**
Methicillin's Impact on Within-Host Dynamics and the Effects of Key Parameters on R_W When $m = 0$ and $m = 1$	• Methicillin ($m = 1$) increases populations of co-infected cells (E_6), SARS-CoV-2 virus (V_2), and MRSA bacteria (B_N). • Neutrophil populations (N_3) remain stable with methicillin (unaffected by methicillin). • Infection rate of COVID-19-MRSA uninfected cells by SARS-CoV-2 (ψ_4): This parameter has positive impact on R_W in both cases ($m = 0$ and $m = 1$), and more substantial in the presence of methicillin. • Decay rate of MRSA bacteria in individuals infected with MRSA (d_1): This parameter has significant negative impact on R_W, and greater in the absence of methicillin. • Decay rate of MRSA bacteria in individuals coinfected with COVID-19 and MRSA (d_2): This parameter has significant negative impact on R_W, and greater in the absence of methicillin.
Impact of Vancomycin Effectiveness	• Increasing vancomycin effectiveness from 50% to 90% reduces MRSA populations in individuals infected with MRSA and individuals coinfected with COVID-19 and MRSA but has no significant changes in other cell populations.
Efficacy of Immunomodulatory Antibiotics	• Increasing the efficacy of immunomodulatory antibiotics (σ_3) leads to an increase in neutrophil population (N_3) but has no impacts on other cells.
Impact of Varying β_3 (Coinfection Rate)	• Higher β_3 values increased populations of individuals coinfected with COVID-19 and MRSA (I_{CM}) and cells infected with COVID-19 (E_2), with no impact on other populations at both scales.
Most Influential Parameters Affecting R_B	• Infection rate of COVID-19 (β_1) • Infection rate of MRSA (β_2) • Recovery rate of individuals infected with MRSA (r) • Isolation rate of individuals infected with COVID-19 (a)

pathogens like COVID-19 [75]. As such, studying the impact of this antibiotics on coinfection dynamics is relevant to real-world clinical scenarios and can provide insights into potential treatment strategies. Also the choice of vancomycin is supported by Mikkaichi et al [50], that have explored their efficacy and mechanisms of action in the context of MRSA infections. Our choice to focus on methicillin in this study is based on its widespread use during the COVID-19 pandemic, the emergence of MRSA strains and the challenges posed by methicillin-resistant staphylococcus aureus [1], [35], [61], [2]. Additionally, investigating the dynamics of methicillin in the context of COVID-19 and MRSA coinfection contributes to addressing the complex interactions between these pathogens and optimizing treatment approaches for co-infected patients. The equilibrium and basic reproduction number of the multiscale model were studied. Our study encompassed a comprehensive global sensitivity analysis of the epidemiological and within-host components of a multiscale model for COVID-19 and MRSA coinfection. For the epidemiological part, the global sensitivity analysis employed Latin Square Sampling and Partial Rank Correlation Coefficient (PRCC) methods, utilizing a sample size of 5000. Figures (3a) and (3b) display PRCC values, revealing that certain factors significantly impact R_B. Parameters such as the infection rate of MRSA (β_2), infection rate of COVID-19 (β_1), recovery rate of MRSA-infected individuals (r), isolation rate of COVID-19-infected individuals (a), exhibited substantial influence on R_B. The analysis indicated that reducing the infection rates of MRSA and COVID-19, as well as increasing the recovery rate of MRSA-infected individuals and the isolation rate of COVID-19-infected individuals, were the most effective measures for reducing the between-host reproduction number. These measures would lead to a decrease in new infections and a reduction in the duration and number of infectious individuals. Thus, interventions targeting these parameters hold promise for mitigating the spread of COVID-19 and MRSA coinfection.

Furthermore, a global sensitivity analysis assessed parameters' impact on within-host reproduction number (R_W), considering two scenarios: with and without methicillin ($m = 0$ and $m = 1$). Using Latin Hypercube Sampling, we analyzed 5000 samples and plotted scatter plots when $m = 0$ (Subfigure 4a) and PRCCs (Subfigure 4b). Key parameters positively affecting R_W included γ_1, γ_2, κ_2, ε_3, and ψ_4, with methicillin amplifying their impact. Conversely, ζ, d_1, d_2, ρ_3, and ρ_1 had negative effects on R_W, especially pronounced with methicillin. These findings underscore the role of methicillin in parameter influence on R_W and stress the importance of tailored strategies for managing COVID-19 and MRSA coinfections amidst antibiotic resistance concerns. Efforts should be made to boost the effectiveness of antibiotics, such as methicillin or alternatives, to further suppress bacterial growth. Controlling parameters like κ_2, ε_3, and ψ_4 is crucial for effective co-infection management. In cases where methicillin is not used ($m = 0$), it is suggested to implement strategies aimed at reducing the intrinsic growth rates of MRSA. This can include infection control measures and prudent antibiotic use. Further, targeting the decay rates of MRSA bacteria in individuals infected with MRSA and individuals coinfected with COVID-19 and MRSA (d_1 and d_2), can further contribute to lowering the within-host reproduction number (R_W).

For numerical simulations results, Figures 5 and 6 display within-host dynamics in COVID-19 and MRSA coinfected individuals (I_{CM}) and MRSA-infected individuals (I_M) after methicillin treatment. In I_{CM}, methicillin ($m = 1$) boosts co-infected cell populations (E_6), SARS-CoV-2 virus (V_2), and MRSA bacteria (B_N) while reducing methicillin-sensitive staphylococcus aureus (B_2). Neutrophil populations (N_3) remain stable, unaffected by methicillin in Figure 5, but in Figure 6, neutrophils in I_M (N_2) slightly rise with methicillin. Figure 7 shows no differences in COVID-19-infected individuals (I_C), viral load (V_1), and infected cells (E_2) between $m = 0$ and $m = 1$, emphasizing methicillin's stronger impact on bacteria. Figure 8 demonstrates a slight increase in MRSA-infected individuals (I_M), co-infected individuals (I_{CM}), environmental MRSA (B_E), and isolated individuals (J) with methicillin ($m = 1$),

but methicillin does not alter populations of individuals infected with COVID-19 (I_C) or environmental virus (V_E). We also evaluated vancomycin's effect on MRSA and COVID-19-MRSA coinfection. Figure 9 reveals decreased MRSA populations in I_M (B_M) and I_{CM} (B_N) with increasing vancomycin effectiveness, and no changes in other cell populations at the within-host scale. In Figure 10, simulations of coinfection dynamics with immunomodulatory antibiotics, show increased neutrophil populations (N_3) without affecting other cells at the within-host scale. These findings guide treatment strategies for COVID-19 and MRSA coinfections while considering antibiotic resistance concerns. Figure 11 explores the impact of varying the coinfection rate (β_3) of COVID-19 and MRSA. At the between-host level, higher β_3 increases coinfected individuals (I_{CM}) without affecting other populations. Within-host, β_3 elevation boosts infected COVID-19 cell counts (E_2) but lowers them with lower values. SARS-CoV-2 virus (V_1) rises slightly with higher β_3 but doesn't affect other within-host cells. These findings highlight the sensitivity of coinfection dynamics to β_3 changes, emphasizing the importance of simultaneous infection control. The study emphasizes the importance of continuous research, surveillance, and the development of effective strategies to combat the complexities of COVID-19 and MRSA coinfection.

Acknowledgements
Some of the authors (TF, CC, AP and RE) acknowledge funding by the MODCOV19 platform of the National Institute of Mathematical Sciences and their Interactions (CNRS).

Funding Statement:
This research was funded by the MODCOV19 platform of the National Institute of Mathematical Sciences and their Interactions (CNRS).

References

[1] J. R. Adalbert, R. Jenna, K. Varshney, R. Tobin and R. Pajaro, *Clinical outcomes in patients co-infected with COVID-19 and Staphylococcus aureus: a scoping review*, BMC Infectious Diseases **21**(2021), 1–17.

[2] S. Aslam, H. Asrat, R. Liang, W. Qiu, S. Sunny, A. Maro, M. Abdallah, M. Fornek, B. Episcopia and J. Quale, *Methicillin-resistant Staphylococcus aureus bacteremia during the coronavirus disease 2019 (COVID-19) pandemic: trends and distinguishing characteristics among patients in a healthcare system in New York City*, Infection Control and Hospital Epidemiology **44**(2022), 1–3.

[3] R. Anderson, G. Tintinger, R. Cockeran, M. Potjo and C. Feldman, *Beneficial and harmful interactions of antibiotics with microbial pathogens and the host innate immune system*, Pharmaceuticals **3** (2010), 1694–1710.

[4] S. Ansari, J. P. Hays, A. Kemp, R. Okechukwu, J. Murugaiyan, M. D. Ekwanzala, M. J. R. Alvarez et al., *The potential impact of the COVID-19 pandemic on global antimicrobial and biocide resistance: an AMR Insights global perspective*, JAC-Antimicrobial Resistance **3**(2021): dlab038.

[5] Y. Alimohamadi, M. Sepandi, M. Taghdir and H. Hosamirudsari, *Determine the most common clinical symptoms in COVID-19 patients: a systematic review and meta-analysis*, Journal of Preventive Medicine and Hygiene **61**(2020): E304.

[6] M. O. Adewole, A. A. Onifade, F. A. Abdullah, F. Kasali and A. I. M. Ismail, *Modeling the Dynamics of COVID-19 in Nigeria.* International Journal of Applied and Computational Mathematics **7**(2021), 1–25.

[7] R. Bekker, M. U. H. Broek, and G. Koole, *Modeling COVID-19 hospital admissions and occupancy in the Netherlands*, European Journal of Operational Research, **304**(2023): 207–218.

[8] B. Acay, M. Inc, A. Khan and A. Yusuf, *Fractional methicillin-resistant Staphylococcus aureus infection model under Caputo operator*, Journal of Applied Mathematics and Computing **67**(2021), 755–783.

[9] B. Selenne, H. Gulbudak, M. A. Horn, Q. Huang, A. Nandi, H. Ryu and R. Segal, *Investigating the impact of combination phage and antibiotic therapy: a modelling study*, in Using Mathematics to Understand Biological Complexity **134**, Springer Cham, 2021, pp. 111–134.

[10] M. Bassetti, L. Magnasco, A. Vena, F. Portunato and D. R. Giacobbe, *Methicillin-resistant Staphylococcus aureus lung infection in coronavirus disease 2019: how common*, Current Opinion in Infectious Diseases **35**(2022), 149-162.

[11] S. Breva, M. Silvia, C. M. Clavero, F.G. Bertomeu, E. Picó-Plana, N. S. Orús, I. P. Sánchez, M. T. Mestre-Prad and M. T. Sans-Mateu, *Evaluation of five immunoassays and one lateral flow immunochromatography for anti-SARS-CoV-2 antibodies detection*, Enfermedades Infecciosasy Microbiologia Clinica (English ed.) **40**(2022), 489–494.

[12] J. Bridges, E. K. Vladar, H. Huang and R. J. Mason, *Respiratory epithelial cell responses to SARS-CoV-2 in COVID-19*, Thorax **77**(2022), 203–209.

[13] S. M. E. K. Chowdhury, J. T. Chowdhury, S. F. Ahmed, P. Agarwal, I. A. Badruddin, and S. Kamangar, *Mathematical modelling of COVID-19 disease dynamics: Interaction between immune system and SARS-CoV-2 within host*, AIMS Mathematics **7**(2022), 2618–2633.

[14] Y. Cheng, S. You, Y. Lin, S. Chen, W. Chen, W. Chou, N. Hsieh, and C. Liao, *Mathematical modeling of post-coinfection with influenza A virus and Streptococcus pneumoniae, with implications for pneumonia and COPD-risk assessment*, International Journal of Chronic Obstructive Pulmonary Disease **12**(2017), 1973–1988.

[15] F. Chamchod and S. Ruan, *Modeling methicillin-resistant Staphylococcus aureus in hospitals: transmission dynamics, antibiotic usage and its history*, Theoretical Biology and Medical Modelling **9**(2012), 1–14.

[16] B. S. Cooper, G. F. Medley, S. P. Stone, C. C. Kibbler, B. D. Cookson, J. A. Roberts, G. Duckworth, R. Lai, and S. Ebrahim, *Methicillin-resistant Staphylococcus aureus in hospitals and the community: stealth dynamics and control catastrophes*, Proceedings of the National Academy of Sciences **101**(2004): 10223–10228.

[17] H. F. Chambers and F. R. DeLeo, *Waves of resistance: Staphylococcus aureus in the antibiotic era.*, Nature Reviews Microbiology **7**(2009), 629–641.

[18] L. dePillis, R. Caffrey, G. Chen, M. D. Dela, L. Eldevik, J. McConnell, S. Shabahang, and S. A. Varvel, *A mathematical model of the within-host kinetics of SARS-CoV-2 neutralizing antibodies following COVID-19 vaccination.*, Journal of Theoretical Biology **556**(2023): 111280.

[19] A. Dalhoff, *Immunomodulatory activities of fluoroquinolones*, Infection **33**, (2005), 55–70.

[20] Data on the daily number of new reported COVID-19 cases and deaths by EU/EEA country, European Centre for Disease Prevention and Control. ecdc.europa.eu/en/publications-data/data-daily-new-cases-covid-19-eueea-country

[21] O. Diekmann, J. A. P. Heesterbeek, and J. A. J. Metz, *On the definition and the computation of the basic reproduction ratio R 0 in models for infectious diseases in heterogeneous populations*, Journal of Mathematical Biology **28**(1990), 365–382.

[22] J. A. C. Delaney, V. Schneider-Lindner, P. Brassard, and S. Suissa, *Mortality after infection with methicillin-resistant Staphylococcus aureus (MRSA) diagnosed in the community*, BMC Medicine **6**(2008), 1–8.

[23] D. Duenas, J. Daza, and Y. Liscano, *Coinfections and Superinfections Associated with COVID-19 in Colombia: A Narrative Review*, Medicina **59**(2023): 1336.

[24] T. S. Faniran, E. A. Bakare, R. Potucek, and E. O. Ayoola, *Global and sensitivity analyses of unconcerned COVID-19 cases in Nigeria: a mathematical modeling approach.*, WSEAS Transactions on Mathematics **20**(2021), 218–234.

[25] T. S. Faniran, L. N. Nkamba, and T. T. Manga, *Qualitative and quantitative analyses of COVID-19 dynamics.*, Axioms **10**(2021): 210.

[26] T. S. Faniran, E. A. Bakare, and A. O. Falade. *The COVID-19 Model with Partially Recovered Carriers*, Journal of Applied Mathematics **21**(2021), 1–17.

[27] European Centre for Disease Prevention and Control (ECDC). Data on the daily number of new reported COVID-19 cases and deaths by EU/EEA country. Data Set. 27 Oct 2022. https://www.ecdc.europa.eu/en/publications-data/data-daily-new-cases-covid-19-eueea-country

[28] France life expectancy 1950-2023, macrotrends.net/countries/FRA/France/life-expectancy (2022).

[29] S. Gao, P. Binod, C. W. Chukwu, T. Kwofie, S. Safdar, L. Newman, S. Choe, et al., *A mathematical model to assess the impact of testing and isolation compliance on the transmission of COVID-19* Infectious Disease Modelling **8**(2023): 427–444.

[30] C. D. Gowler, R. B. Slayton, S. C. Reddy, and J. J. O'Hagan, *Improving mathematical modeling of interventions to prevent healthcare-associated infections by interrupting transmission or pathogens: How common modeling assumptions about colonized individuals impact intervention effectiveness estimates* PLOS ONE **17**(2022): e0264344.

[31] F. E. Guerra, T. R. Borgogna, D. M. Patel, W. E. Sward, and J. M. Voyich, *Epic immune battles of history: neutrophils vs. Staphylococcus aureus*, Frontiers in Cellular and Infection Microbiology **286**(2017).

[32] C. Garcia-Vidal, G. Sanjuan, E. Moreno-García, P. Puerta-Alcalde, N. Garcia-Pouton, M. Chumbita, M. Fernandez-Pittol, et al., *Incidence of co-infections and superinfections in hospitalized patients with COVID-19: a retrospective cohort study*, Clinical Microbiology and Infection **27**(2021), 83–88.

[33] N. Gokbulut, U. Hurdoganoglu, N. Sultanoglu, E. Guler, E. Hincal, and K. Suer, Compartmental Mathematical Model with Optimal Control: Can awareness against Methicillin Resistant Staphylococcus aureus prevent its transmission, Research Square (2023): https://doi.org/10.21203/rs.3.rs-3239004/v1.

[34] Centre for Health Protection, Department of Health, The Government of Hong Kong Special Administrative Region, https://www.chp.gov.hk/en/statistics/data/10/100044/6864.html

[35] G. Habib, K. Mahmood, H. Gul, M. Tariq, Q. U. Ain, A. Hayat, and M. U. Rehman, *Pathophysiology of Methicillin-Resistant Staphylococcus aureus Superinfection in COVID-19 Patients*, Pathophysiology **29**(2022), 405–413.

[36] R. E. W. Hancock, A. Nijnik, and Dana J. Philpott, *Modulating immunity as a therapy for bacterial infections*, Nature Reviews Microbiology **10**(2012), 243–254.

[37] A. Harper, V. Vijayakumar, A. C. Ouwehand, J. T. Haar, D. Obis, J. Espadaler, S. Binda, S. Desiraju, and R. Day, *Viral infections, the microbiome, and probiotics*, Frontiers in Cellular and Infection Microbiology **10**(2021): 596166.

[38] Q. Huang, X. Huo, D. Miller, and S. Ruan, *Modeling the seasonality of methicillin-resistant Staphylococcus aureus infections in hospitals with environmental contamination*, Journal of Biological Dynamics **13**(2019), 99–122.

[39] N. V. Ivanisenko, K. Seyrek, N. A. Kolchanov, V. A. Ivanisenko, and I. N. Lavrik, *The role of death domain proteins in host response upon SARS-CoV-2 infection: modulation of programmed cell death and translational applications*, Cell Death Discovery **6**(2020): 101.

[40] F. Inayaturohmat, N. Anggriani, and A. K. Supriatna, *A mathematical model of tuberculosis and COVID-19 co-infection with the effect of isolation and treatment*, Frontiers in Applied Mathematics and Statistics **8**(2022): 958081.

[41] N. Imai, T. Rawson, E. S. Knock, R. Sonabend, Y. Elmaci, P. N. Perez-Guzman, L. K. Whittles, et al., *Quantifying the effect of delaying the second COVID-19 vaccine dose in England: a mathematical modelling study*, The Lancet Public Health **8**(2023): e174-e183.

[42] K. Jeon, S. Jeong, N. Lee, P. Min-Jeong, W. Song, K. Han-Sung, H. S. Kim, and K. Jae-Seok, *Impact of COVID-19 on antimicrobial consumption and spread of multidrug-resistance in bacterial infections*, Antibiotics **11**(2022): 535.

[43] D. Jonas, M. Speck, F. D. Daschner, and H. Grundmann, *Rapid PCR-based identification of methicillin-resistant Staphylococcus aureus from screening swabs*, Journal of Clinical Microbiology **40**(2002), 1821–1823.

[44] Kumar Rai, Rajanish, Pankaj Kumar Tiwari, and Subhas Khajanchi, *Modeling the influence of vaccination coverage on the dynamics of COVID-19 pandemic with the effect of environmental contamination*, Mathematical Methods in the Applied Sciences **46**(2023): 12425–12453.

[45] M. T. Kashef and Omneya M. Helmy, *Development of a multiplex polymerase chain reaction-based DNA lateral flow assay as a point-of-care diagnostic for fast and simultaneous detection of MRSA and vancomycin resistance in bacteremia*, Diagnostics **12**(2022): 2691.

[46] A. Kramer, I. Schwebke, and G. Kampf, *How long do nosocomial pathogens persist on inanimate surfaces, A systematic review*, BMC Infectious Diseases **6**(2006), 1–8.

[47] Z. S. Kifle, and L. L. Obsu, *Mathematical modeling for COVID-19 transmission dynamics: A case study in Ethiopia*, Results in Physics **34**(2022): 105191.

[48] R. S. Loomba, G. Aggarwal, S. Aggarwal, S. Flores, E. G. Villarreal, J. S. Farias, and C. J. Lavie, *Disparities in case frequency and mortality of coronavirus disease 2019 (COVID-19) among various states in the United States*, Annals of Medicine **53**(2021), 151–159.

[49] A. Langdon, N. Crook, and G. Dantas, *The effects of antibiotics on the microbiome throughout development and alternative approaches for therapeutic modulation*, Genome Medicine **8**(2016), 1–16.

[50] T. Mikkaichi, M. R. Yeaman, A. Hoffmann and MRSA Systems Immunobiology Group, *Identifying determinants of persistent MRSA bacteremia using mathematical modeling*, PLoS Computational Biology **7**, (2019): e1007087.

[51] S. Mallett, A. J. Allen, S. Graziadio, S. A. Taylor, N. S. Sakai, K. Green, J. Suklan, et al, *At what times during infection is SARS-CoV-2 detectable and no longer detectable using RT-PCR-based tests. A systematic review of individual participant data*, BMC Medicine **18**(2020), 1–17.

[52] E. McKenna, R. Wubben, J. M. Isaza-Correa, A. M. Melo, A. U. Mhaonaigh, N. Conlon, J. S. O'Donnell, et al. *Neutrophils in COVID-19: Not innocent bystanders.* Frontiers in Immunology **13**(2022): 2548.

[53] K. G. Mekonen and L. L. Obsu. *Mathematical modeling and analysis for the co-infection of COVID-19 and tuberculosis.* Heliyon **8**(2022): 11195.

[54] Y. Ma, Y. Zhang, and Liuluan Zhu. *Role of neutrophils in acute viral infection.* Immunity, Inflammation and Disease **9**(2021), 1186–1196.

[55] MedlinePlus, Trusted Health Information For You, *MRSA Tests.*, https://medlineplus.gov/lab-tests/mrsa-tests/

[56] A. G. C. Pérez and David Adeyemi Oluyori, *A model for COVID-19 and bacterial pneumonia coinfection with community-and hospital-acquired infections*, Mathematical Modelling and Numerical Simulation with Applications **4**(2022), 197–210.

[57] F. K. Mbabazi, J. Y. T. Mugisha, and M. Kimathi, *Modeling the within-host co-infection of influenza A virus and pneumococcus*, Applied Mathematics and Computation **339**(2018), 488–506.

[58] F. Ndairou, I. Area, J. J Nieto, and D. F. M. Torres, *Mathematical modeling of COVID-19 transmission dynamics with a case study of Wuhan*, Chaos, Solitons and Fractals **135**(2020): 109846.

[59] C. Osterholzer, O. Zhang, C. Huffnagle, and Toews, *Accumulation of CD11b Neutrophils in response to fungal infection is critical for host defence*, Immunity **89**(2017), 1363–1374.

[60] J. Pillay, I. D. Braber, N. Vrisekoop, L. M. Kwast, R. J. De Boer, J. AM Borghans, K. Tesselaar, and L. Koenderman, *In vivo labeling with 2H2O reveals a human neutrophil lifespan of 5.4 days*, The Journal of the American Society of Hematology **116**(2010), 625–627.

[61] C. D. Punjabi, T. Madaline, I. Gendlina, V. Chen, P. Nori, and P. Liise-anne, *Prevalence of methicillin-resistant Staphylococcus aureus (MRSA) in respiratory cultures and diagnostic performance of the MRSA nasal polymerase chain reaction (PCR) in patients hospitalized with coronavirus disease 2019 (COVID-19) pneumonia*, Infection Control and Hospital Epidemiology **42**(2021), 1156–1158.

[62] D. V. Patangia, V. Dhrati, C. A. Ryan, E. Dempsey, P. R. Reynolds, and C. Stanton, *Impact of antibiotics on the human microbiome and consequences for host health*, MicrobiologyOpen **11**(2022): e1260.

[63] M. J. Parnham, *Immunomodulatory effects of antimicrobials in the therapy of respiratory tract infections*, Current Opinion in Infectious Diseases **18**(2005), 125–131.

[64] A. G. C. Pérez and D. A. Oluyori, *A model for COVID-19 and bacterial pneumonia coinfection with community-and hospital-acquired infections*, arXiv preprint arXiv **2**(2022).

[65] L. R. W. Plano, A. C. Garza, T. Shibata, S. M. Elmir, J. Kish, C. D. Sinigalliano, M. L. Gidley, et al., *Shedding of Staphylococcus aureus and methicillin-resistant Staphylococcus aureus from adult and pediatric bathers in marine waters*, BMC Microbiology **11**(2011), 1–10.

[66] Y. Roche, M. Fay, and Marie-Anne Gougerot-Pocidalo, *Effects of quinolones on interleukin 1 production in vitro by human monocytes*, Immunopharmacology **13**(1987), 99–109.

[67] J. D. Ramirez, C. Maldonado, and C. Jaramillo, *A mathematical model of the interaction between influenza A virus and Streptococcus pneumoniae co-infection dynamics*, Journal of Theoretical Biology **458**(2018), 57–68, https://doi.org/10.1016/j.jtbi.2018.09.005.

[68] H. K-A, Ramadan, M. A. Mahmoud, M. Z. Aburahma, A. A. Elkhawaga, M. A. El-Mokhtar, I. M. Sayed, A. Hosni, S. M. Hassany, and M. A. Medhat, *Predictors of severity and co-infection resistance profile in COVID-19 patients: First report from upper Egypt*, Infection and Drug Resistance **20**, (2020), 3409–3422.

[69] S. Rezasoltani, A. Yadegar, B. Hatami, H. A. Aghdaei, and M. Z. Zali, *Antimicrobial resistance as a hidden menace lurking behind the COVID-19 outbreak: the global impacts of too much hygiene on AMR*, Frontiers in Microbiology **11**(2020): 590683.

[70] M. Sadria and T. L. Anita, *Modeling within-host SARS-CoV-2 infection dynamics and potential treatments*, Viruses **13**(2021): 1141.

[71] A. Saltelli, S. Tarantola, and F. Campolongo, *Sensitivity analysis as an ingredient of modeling*, Statistical Science **20**(2000), 377–395.

[72] S. Stefani, D. R. Chung, and J. A. Lindsay, *Methicillin-resistant Staphylococcus aureus (MRSA): Mechanisms of virulence and resistance*, International Journal of Antimicrobial Agents, **61**(2012), 273–282.

[73] E. R. Ulloa and G. Sakoulas, *Azithromycin: An underappreciated quinolone-sparing oral treatment for Pseudomonas aeruginosa infections*, Antibiotics **11**(2022): 515.

[74] M. Sadria and A. T. Layton, *Modeling within-host SARS-CoV-2 infection dynamics and potential treatments*, Viruses **13**(2021): 1141.

[75] J. Tang, H. Jiali, L. Kang, Z. Deng, J. Wu, and J. Pan, *The use of vancomycin in the treatment of adult patients with methicillin-resistant Staphylococcus aureus (MRSA) infection: a survey in a tertiary hospital in China*, International Journal of Clinical and Experimental Medicine **8**(2015): 19436.

[76] D. Tian, Z. Lin, E. M. Kriner, D. J. Esneault, J. Tran, J. C. DeVoto, N. Okami, et al, *Ct values do not predict severe acute respiratory syndrome coronavirus 2 (SARS-CoV-2) transmissibility in college students*, The Journal of Molecular Diagnostics **23**(2021), 1078–1084.

[77] V. Gisbergen, P. J. M. Klaas, M. Sanchez-Hernandez, T. BH Geijtenbeek, and Y. V. Kooyk, *Neutrophils mediate immune modulation of dendritic cells through glycosylation-dependent interactions between Mac-1 and DC-SIGN*, Journal of Experimental Medicine **201**(2005), 1281–1292.

[78] X. Wang, S. Wang, J. Wang, and L. Rong, *A Multiscale Model of COVID-19 Dynamics*, Bulletin of Mathematical Biology **84**(2022), 1–41.
[79] J. B. Xavier, J. M. Monk, S. Poudel, C. J. Norsigian, A. V. Sastry, C. Liao, J. Bento, et al., *Mathematical models to study the biology of pathogens and the infectious diseases they cause*, iScience **25**(2022): 104079.
[80] Y. Zhou, M. Huang, Y. Jiang, and X. Zou, *Data-driven mathematical modeling and dynamical analysis for SARS-CoV-2 coinfection with bacteria*, International Journal of Bifurcation and Chaos **31**(2021): 2150163.
[81] L. Wang, Y. Liang, M. Li, L. Zhang, J. Qi, P. Li, L. Liang, *Neutrophil-based SARS-CoV-2 clearance contributes to the pathogenesis of COVID-19*, Signal Transduction and Targeted Therapy **81**(2022), 1–11. doi: 10.1038/s41392-021-00854-0
[82] X. Wang, Y. Xiao, J. Wang, and X. Lu., *A mathematical model of effects of environmental contamination and presence of volunteers on hospital infections in China*, Journal of Theoretical Biology **293**(2012), 161–173.
[83] Y. Wang, N. Chitnis, and E. Fairbanks, *Optimizing malaria vector control: A systematic review and mathematical modelling study to identify desirable characteristics of novel tools in different settings*, Preprint (2023).
[84] R. Wölfel, V. M. Corman, W. Guggemos, M. Seilmaier, S. Zange, M. A. Müller, D. Niemeyer et al., *Virological assessment of hospitalized patients with COVID-2019*, Nature **581**(2020), 465–469.
[85] World Data Atlas, *France Demographics Knoema*, com/atlas/France/population
[86] World data atlas, *France total population; France demographics*, knoema.com/atlas/France/population (2022)
[87] L.F. Westblade, M.S. Simon and M.J. Satlin, *Bacterial coinfections in coronavirus disease 2019*, Trends In Microbiology **29**(2021), 930–941.
[88] X. Wang, S. Wang, J. Wang and L. Rong, *A Multiscale Model of COVID-19 Dynamics*, Bulletin of Mathematical Biology **84**(2022), 1–41.

T. Faniran, corresponding author, LmB, CNRS, Universite de Franche-Comte, F-25000 Besancon, France
Current address: Department of Computer Science, Lead City University, Ibadan, Nigeria
Email address: faniran.taye@univ-fcomte.fr

M. O. Adewole, School of Mathematical Sciences, Universiti Sains Malaysia, Malaysia
Current address: Department of Computer Science and Mathematics, Mountain Top University, Prayer City, Ogun State, Nigeria
Email address: olamatthews@ymail.com

C. Chirouze, CHU Besancon, CNRS, Chrono-environment, Universite de Franche-Comte, F-25000 Besancon, France
Email address: catherine.chirouze@univ-fcomte.fr

A. Perasso, Chrono-environment, CNRS, Universite de Franche-Comte, F-25000 Besancon, France
Email address: antoine.perasso@univ-fcomte.fr

R. Eftimie, LmB, CNRS, Universite de Franche-Comte, F-25000 Besancon, France
Email address: raluca.eftimie@univ-fcomte.fr